frontiers | Frontiers in Earth Science

TYPE Original Research
PUBLISHED 05 June 2025
DOI 10.3389/feart.2025.1572864

Termination of rapid exhumation of the Jiaodong Peninsula during the Early Cretaceous: implications for explosive gold mineralization

Jianweng Gao, Keqiang Zhao*, Zhuang Duan, Yangang Fu, Lujun Lin, Zhenliang Wang, Jingjing Gong, Jianzhou Yang and Yong Li*

State Key Laboratory of Deep Earth and Mineral Exploration, Institute of Geophysical and Geochemical Exploration, Chinese Academy of Geological Sciences, Tianjin, China

OPEN ACCESS

EDITED BY
KunFeng Qiu,
China University of Geosciences, China

REVIEWED BY
Fangyang Hu,
Institute of Geology and Geophysics (CAS), China
Peng Chai,
Institute of Geology, Chinese Academy of Geological Sciences (CAGS), China

*CORRESPONDENCE
Keqiang Zhao,
zkeqiang@mail.cgs.gov.cn
Yong Li,
cgslyong@mail.cgs.gov.cn

RECEIVED 07 February 2025
ACCEPTED 26 May 2025
PUBLISHED 05 June 2025

CITATION
Gao J, Zhao K, Duan Z, Fu Y, Lin L, Wang Z, Gong J, Yang J and Li Y (2025) Termination of rapid exhumation of the Jiaodong Peninsula during the Early Cretaceous: implications for explosive gold mineralization.
Front. Earth Sci. 13:1572864.
doi: 10.3389/feart.2025.1572864

The proven gold deposits in the Jiaodong Peninsula, North China Craton, exceed 5,500 tons; these deposits are termed “Jiaodong type” or “Craton destruction type” owing to their unique geological features. Metallogenic chronology has dated the formation of these deposits at 120 ± 2 Ma. The development of such significant gold deposits in a relatively short period can be characterized as “explosive gold mineralization” and its driving factors are still under investigation. To clarify the geochemical characteristics, genesis and thermal history of a newly discovered quartz monzodiorite in the Tianqishan area, Shandong Province and their relationship with gold mineralization, the geochemistry of major and trace elements, zircon U–Pb isotope chronology, zircon Hf isotopes, and apatite fission track (AFT) thermochronology are analyzed. Our results show that the Tianqishan quartz monzodiorite, emplaced at ca. 119 Ma, is a metaluminous, high-K calc-alkaline rock, formed by mixing of mantle and crustal melts in a tectonic setting of North China Craton thinning. The AFT thermal history modeling results reveal four cooling events since the formation of the Tianqishan quartz monzodiorite and affirm two extensional stages in the Jiaodong Peninsula during the Early Cretaceous. The rapid exhumation of the crust of the Jiaodong Peninsula terminated at approximately ca. 120 ± 2 Ma, which may be due to the decoupling between crustal detachment and lithospheric mantle detachment in the Jiaodong Peninsula. Notably, the explosive mineralization of gold deposits aligns with the end of rapid exhumation in the Early Cretaceous, suggesting that decoupling between crustal and lithospheric mantle detachment is a plausible explanation for this phenomenon. This study provides critical new insights into the geodynamic processes governing Early Cretaceous lithospheric thinning and offers key constraints on the mechanisms driving explosive gold mineralization in the Jiaodong Peninsula.

KEYWORDS

Jiaodong Peninsula gold deposits, the early cretaceous, explosive gold mineralization, apatite fission track (AFT), termination of rapid exhumation

1 Introduction

The Jiaodong Peninsula is located in the southeastern margin of the North China Craton. The region underwent Triassic continental collision, followed by Early Jurassic subduction of the Paleo-Pacific Plate, making it an ideal location to study subduction–collision processes and craton destruction. Additionally, the proven gold deposits in the Jiaodong Peninsula amount to more than 5,500 tons, and some scientists refer to this area as the Jiaodong gold province (Deng et al., 2022; Qiu et al., 2024b). The Jiaodong gold province, formed in a cratonic destruction setting, is distinct from other significant giant gold provinces worldwide, such as Carlin in the United States, Muruntau in Uzbekistan, and Witwatersrand in South Africa. Consequently, it has been classified as "Jiaodong type" (Zhai et al., 2004; Deng et al., 2015) or "Decratonic gold deposits" (Zhu et al., 2015). Many researchers have made great achievements in tectonic setting (Zhu et al., 2015; Zhu and Sun, 2021; Deng et al., 2022; Qiu et al., 2023a; Song et al., 2023; Yang et al., 2024; Wang et al., 2025a; Yao et al., 2025), metallogenic epoch (Ma et al., 2017; Li et al., 2018a; Yang et al., 2018; Deng et al., 2020; Li et al., 2025), ore-forming material source (He et al., 2024; Qiu et al., 2024a; Wang et al., 2025a; Zhang et al., 2024), migration precipitation of ore-forming fluid (Chai et al., 2017; Chai et al., 2019c; Chai et al., 2019b; Chai et al., 2019a; Kuang et al., 2025; Wang et al., 2025b), gold precipitation (Fan et al., 2003; Goldfarb and Santosh, 2014; Wang et al., 2015; Wen et al., 2015; Du et al., 2025) and exhumation of mineral bodies after mineralization (Li et al., 2018b; Wu et al., 2018; Yang et al., 2020; Zhang et al., 2022; Qiu et al., 2023b). With the application of increasingly precise geochronological methods, researchers have established that the mineralization age of the gold deposits in the Jiaodong Peninsula is concentrated in 120 ± 2 Ma (Deng et al., 2020). The development of such significant gold deposits in a relatively short period can be characterized as "explosive gold mineralization." However, the controlling factors of "explosive gold mineralization" are still controversial. Although it is widely recognized that the gold deposits in the Jiaodong Peninsula are related to the subduction of the subduction of the Palaeo-Pacific plate, and the destruction of the North China Craton (Zhu et al., 2015; Zhu and Xu, 2019; Deng et al., 2022), how to regulate the contradiction between the long-term enrichment of mineralizing elements and the concentrated release in a short period of time still requires further research (Deng et al., 2020).

In recent years, lots of thermochronological studies have been conducted in the Jiaodong Peninsula (Liu et al., 2017; Gao and Li, 2020; Sun et al., 2022; Zhang et al., 2022; Qiu et al., 2023b), which provide thermal history constraints for the genesis of gold deposits in the Jiaodong Peninsula. However, the ore-forming temperature for the Jiaodong gold deposits is about 220°C–304°C (Fan et al., 2003; Goldfarb and Santosh, 2014; Wang et al., 2015; Wen et al., 2015), which overlaps with the closure temperature determined via the zircon fission track (ZFT) (240°C ± 50°C) method and are higher than the closure temperature range determined via the apatite fission track (AFT) method (60°C–120°C) (Reiners and Brandon, 2006). It is speculated that rocks affected by gold mineralization hydrothermal activities may undergo annealing or partial annealing. This leads to the fact that numerous low-temperature thermochronology findings can effectively constrain the post-gold-mineralization thermal history of the Jiaodong Peninsula, while insufficiently constrain the thermal history of the mineralization period.

The gold mineralization on the Jiaodong Peninsula is closely related to Mesozoic granites. The Late Jurassic Linglong and Guojialing granites are the major ore-hosted rocks of the Jiaodong gold deposits (Feng et al., 2022). However, the Early Cretaceous Weideshan granites, which have emplacement ages that overlap with the time of gold mineralization, do not contain mineralized gold. Consequently, the Weideshan suite is ideal for studying the regional cooling history during the Jiaodong Peninsula's gold mineralization period. Meanwhile, the contrasting mineralisation mechanisms between the ore-hosted granites and the Weideshan suite may also provide a basis for exploring the "explosive gold mineralization" in the Jiaodong Peninsula.

In this study, we investigated geochemistry, zircon U–Pb isotope chronology and AFT thermochronology of a newly discovered quartz monzodiorite from the Tianqishan area, which lacks gold mineralization. The aim was to elucidate the geochemical characteristics, and genesis of the intrusion, and simulate its thermal history. These findings provide new insights into and constraints on Early Cretaceous "explosive gold mineralization" on the Jiaodong Peninsula.

2 Geological setting

The Jiaodong Peninsula is situated at the southeastern margin of the North China Craton and is bounded by the Tan-Lu Fault to the west (Qiu et al., 2023a). It is divided by the Wulian–Yantai Fault into the Sulu Orogenic Belt to the southeast and the Jiaobei Terrane to the northwest (Figure 1a). The Sulu Orogenic Belt originated during the Middle to Late Triassic and consists of metamorphic rocks that underwent high-pressure and ultrahigh-pressure metamorphism, along with Mesozoic intrusive rocks (Long et al., 2025b). The Jiaobei Terrane is composed mainly of Precambrian metamorphic basement and Late Mesozoic intrusions (Hacker et al., 2009; Xu et al., 2009; Chai et al., 2020a; Chai et al., 2020b; Chen et al., 2025; Fang et al., 2025; Wang et al., 2025c; Liu et al., 2025; Wang et al., 2025a; Yao et al., 2025). The southwestern part of the Jiaodong Peninsula is covered by the Jiaolai Basin, which consists of Cretaceous volcanic and terrigenous clastic rocks [the Laiyang Formation (K_1l, 131–123 Ma), the Qingshan Formation (K1*q*, 122–100 Ma), and the Wangshi Formation (K_2w, 85–65 Ma)] (Zhang et al., 2003; Ni et al., 2016; Cui et al., 2025). The Jiaolai Basin is also a detachment basin for the Linglong (Charles et al., 2011; Charles et al., 2013; Wu et al., 2020), Queshan (Xia et al., 2016), and Wulian (Ni et al., 2013; Ni et al., 2016) metamorphic core complexes (MCCs). The rapid uplift of these three MCCs indicates a strong extensional tectonic setting in the Jiaodong Peninsula during the Late Mesozoic.

The Jiaodong Peninsula experienced significant magmatism during the Late Mesozoic, resulting in the formation of four main types of intrusive rocks: the Late Jurassic Linglong granites (164 ± 2 to 140 ± 4 Ma), the Early Cretaceous Guojialing granites (130 ± 3 to 125.4 ± 2.2 Ma), the Early Cretaceous Weideshan granites (126 ± 3 to 108 ± 2 Ma), the Laoshan granites (120 ± 2 to 107.0 ± 2.1 Ma), and the Early Cretaceous basic dykes and veins (121.6 ± 1.7 to 114 ± 2 Ma) (Sai and Qiu, 2020; Song et al., 2020b; Song et al., 2022). These magmatic rocks are related to the subduction of the

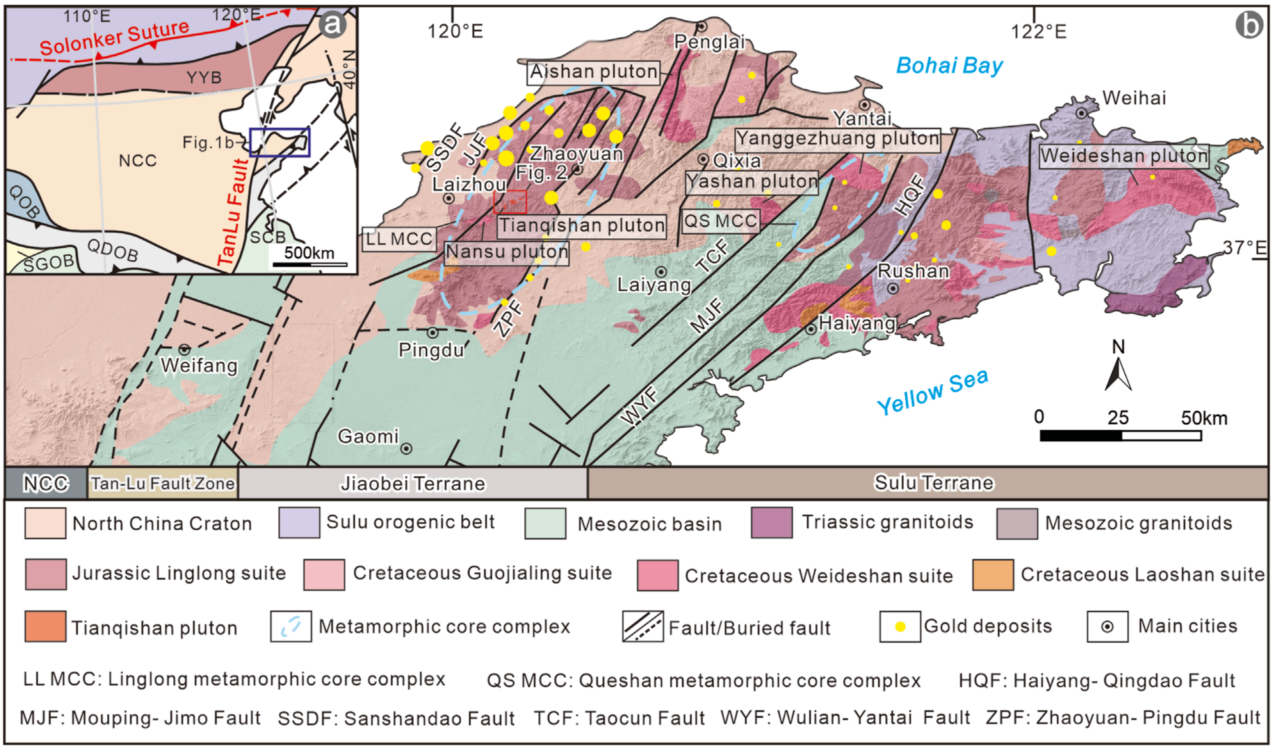

FIGURE 1
(a) Tectonic schematic of East China, showing the location of the Jiaodong Peninsula; **(b)** geological map of the Jiaodong Peninsula, with the study sites marked, showing major structures and lithological units, modified after Song et al. (2018) and Qiu et al. (2024a).

Paleo–Pacific plate and the destruction of the North China Craton. The Late Jurassic Linglong granites are distributed mainly in the northern part of the Jiaobei Terrane and the northern part of the Sulu Orogenic Belt. The Early Cretaceous magmatic rocks are distributed throughout the Jiaodong Peninsula, among which the Early Cretaceous Guojialing granites are distributed mainly in the Jiaobei Terrane, and the Early Cretaceous Weideshan granites have a wider range of distribution, and can be found in Weideshan, Sanfoshan, Haiyang, Yashan, Nanshu, and Laoshan (Figure 1b). From the Jurassic to the Early Cretaceous, the changes in the geochemical compositions of these three stages of granites indicate that the mantle switched from enriched to depleted (Liu et al., 2004; Yan et al., 2005; Yang et al., 2012; Song et al., 2017; Wang et al., 2021; Wang et al., 2022).

The Tianqishan quartz monzodiorite is located in the core of the Linglong MCC and intrudes into the Linglong granite as a stock (Figures 1b, 3a). Due to quarrying activities, it is exposed with an area of less than 1 km^2. There are also stocks of diorites in the east and northeast of the Tianqishan quartz monzodiorite (Figure 2). Some studies collectively refer to them as Zhouguan diorites, with an emplacement age of approximately 118 Ma ±119 Ma (Wang et al., 2024a). Judging from their occurrence and emplacement age, the Tianqishan quartz monzodiorite and the Zhouguan diorite should be the products of homologous magma emplacement. These intrusive rocks, in conjunction with the Nansu pluton to the south and the Aishan pluton to the north (Figure 1b), are all categorised as part of the Weideshan Suite (Wang et al., 2024b).

3 Samples and methods

We collected fresh, unaltered rock samples and from the locations shown in Figure 2. Mafic microgranular enclaves (MMEs) can be observed in the rocks (Figure 3b) and there are potassic alterations and metallic sulfide minerals (pyrite) along joints and fractures (Figure 3c). However, there is no evidence of gold mineralization. Major and trace element analyses were performed on both samples. Additionally, zircon U–Pb isotopes, Hf isotopes and AFT analyses were conducted on sample SQ01.

With medium-to fine-grained textures and massive structures, the dark gray samples we collected are composed mainly of plagioclase (55–60 vol%), K-feldspar (10–15 vol%), quartz (10–15 vol%), hornblende (10–15 vol%) and biotite (3–5 vol%). In addition, the accessory minerals are mainly zircon, magnetite and apatite. Plagioclase, with particle sizes of 2–4 mm, has a hypidiomorphic platy shape, surficial sericitization, polysynthetic twins, and a zonal texture. K-feldspars have xenomorphic platy shapes with particle sizes of 2–3 mm. The green-colored hornblende has an allotriomorphic columnar shape with particle sizes of 0.5–2.2 mm, and pleochroism can be observed. With particle sizes of 0.5–2.2 mm, the ochre-colored biotite exhibits a flaky shape, and some are distributed inside the feldspar crystals. The quartz has an allotriomorphic granular shape, with particle sizes of 2–4 mm (Figure 3d). According to the characteristics observed under a microscope, the intrusive rock should have been quartz monzodiorite.

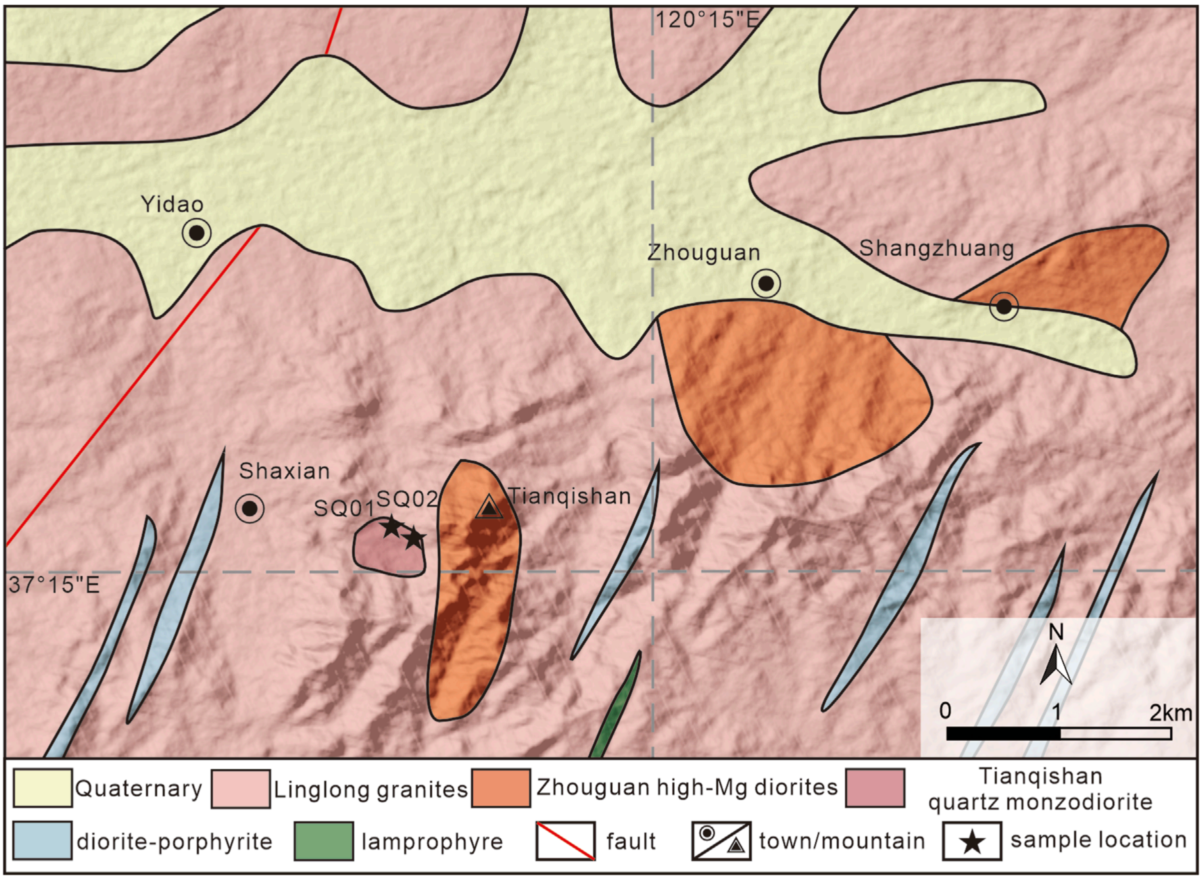

FIGURE 2
Geological map of the Tianqishan area and the locations of the samples.

3.1 Major and trace elements

The geochemical analysis of the samples was completed at the Hebei Provincial Regional Geological Survey Research Institute. Major element analysis was conducted via X-ray fluorescence (XRF) spectrometry on an Axiosmax X-ray fluorescence spectrometer. Rare earth elements and trace elements were determined via inductively coupled plasma-mass spectrometry (ICP–MS; X-Series 2). The laboratory conditions for the experiment were a temperature of 20°C and a humidity of 30%. The results of the major and trace element analyses can be found in Supplementary Table S1.

3.2 LA–ICP–MS zircon U–Pb isotopes and *in situ* Hf isotopes

Zircon selection was completed in the Hebei Provincial Regional Geological Survey Research Institute laboratory. After routine screening, zircons with a purity of more than 99% were manually picked under a binocular microscope. The selected zircons were intact and highly transparent.

The picked zircons were then pasted onto an epoxy resin surface, ground, and polished to expose the zircon surface, creating a target sample. Transmission, reflected light, and cathodoluminescence (CL) images of the zircons were obtained at the Beijing Zircon Navigation Technology Co., Ltd., laboratory, via a JSM6510 scanning electron microscope (JEOL, Inc.).

Zircon U–Pb isotopes and *in situ* Hf isotopes analyses were completed in the laboratory of Tianjin Geological Survey Center of China Geological Survey. A Neptune instrument (Thermo Fisher Scientific, Inc.) was used. The specific instrument configuration and experimental process are described in the literature refer to Li et al. (2009) and Geng et al. (2011). U–Pb isotopes and Hf isotopes data were processed via the ICPMS DataCal program (Liu et al., 2009a; Liu et al., 2010; Hu et al., 2012).

3.3 AFT

AFT ages were obtained via the LA-ICP-MS method (Hasebe et al., 2004) and calculated via the zeta calibration method (Pang et al., 2017) at the Institute of Geology, China Earthquake Administration. The age calibration standard was Durango apatite (31.4 ± 0.5 Ma). The National Bureau of Standards trace element glass NIST612 was used as an external standard to measure the signal intensity during testing. Uranium measurements were carried out with LA–ICPMS equipment. Spontaneous fission tracks in apatite were etched in 5.5 M HNO_3 at 21°C for 20 s. Fission tracks and track length measurements

FIGURE 3
(a) Photograph taken in the field, showing the relationship between the Tianqishan quartz monzodiorite and Linglong granites; **(b)** pyrite and potassic alteration in the Tianqishan quartz monzodiorite; **(c)** MMEs in the Tianqishan quartz monzodiorite; **(d,e)** photomicrograph of the Tianqishan quartz monzodiorite under cross-polarized light (XPL); **(f)** photomicrograph of the Tianqishan quartz monzodiorite under plane-polarized light (PPL), corresponding to **(e)**. Bt: biotite; Hbl: hornblende; Kfs: K-feldspar; Pl: plagioclase; and Qtz: quartz.

were performed on a Zeiss Axioplan2 microscope using a dry objective with a magnification of 1,000×. All AFT analyses were performed by J. Z. Pang, whose laboratory had a weighted mean zeta of Apatite-Zeta NIST612 = 1940 ± 50, while the above methods and standards were used.

4 Results

4.1 Major and trace elements

According to the SiO_2 contents (57.47 wt%–57.97 wt%) of the rocks, the rocks should be classified as intermediate rocks. The rocks have Al_2O_3 contents ranging from 16.08 wt% to 16.57 wt%, and the total alkali contents ($Na_2O + K_2O$) range from 6.27 wt% to 6.37 wt%. The ratios of Na_2O to K_2O are between 1.28 and 1.43. The TFe_2O_3 contents range from 5.38 wt% to 5.87 wt%. The MgO contents are between 4.44 wt% and 4.89 wt% and the $Mg^{\#}$ values range from 59.42–59.69; thus, the Tianqishan quartz monzodiorite is high-Mg diorite (Chen et al., 2013) On the basis of the SiO_2-K_2O diagram, the samples are classified as belonging to the high-potassium calc-alkaline series (Figure 4). In the A/CNK–A/NK diagram, the samples are located within the metaluminous field (Figure 5). The Rittmann index σ_{43} values are between 2.71 and 2.72, indicating that the rock is calc-alkaline. The major element oxides (SiO_2, MgO, TFe_2O_3, CaO, TiO_2, and P_2O_5) are clearly negatively correlated with the SiO_2 content (Figure 6), suggesting significant fractional crystallization of minerals, such as feldspar, pyroxene, amphibole, apatite, and ilmenite.

The Tianqishan quartz monzodiorite has total rare earth element (REE) contents ranging from 189.9×10^{-6} to 239.4×10^{-6}. Light rare earth elements (LREEs) are dominant, with contents varying from 179.14×10^{-6} to 225.74×10^{-6}, whereas heavy rare earth elements (HREEs) are less abundant, ranging from 11.02×10^{-6} to 13.88×10^{-6}. The ratios of LREEs to HREEs (LREEs/HREEs) are consistently between 16.256 and 16.264, and the $(La/Yb)_N$ ratios fluctuate between 24.54 and 26.32, indicating pronounced fractionation between light and heavy rare earth elements (Figure 7a). The REE patterns of the Tianqishan quartz monzodiorite are characterized by an enrichment in LREEs and a depletion in HREEs, manifesting as a right-leaning pattern (Figure 7a). The REE distribution pattern shows a gradual decrease in the content of LREEs and an almost horizontal trend for the content of HREEs. The europium anomaly values, represented by δ_{Eu} values, range from 0.97 to 1.12, suggesting the absence of a Eu anomaly or a slight positive anomaly.

In the primitive mantle-normalized trace element spider diagram, the overall curve exhibits a right-leaning characteristic,

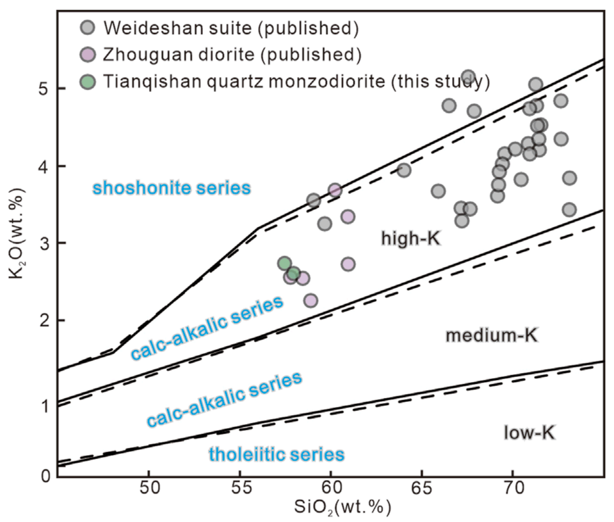

FIGURE 4
K_2O *versus* SiO_2 diagram showing the subdivisions of Le Maitre (1989) (dashed lines and black text) and Rickwood (1989) (blue text). The published data mentioned here and below were obtained from Song et al. (2020b), Wang et al. (2024a), Li et al. (2012) and Wang et al. (2023).

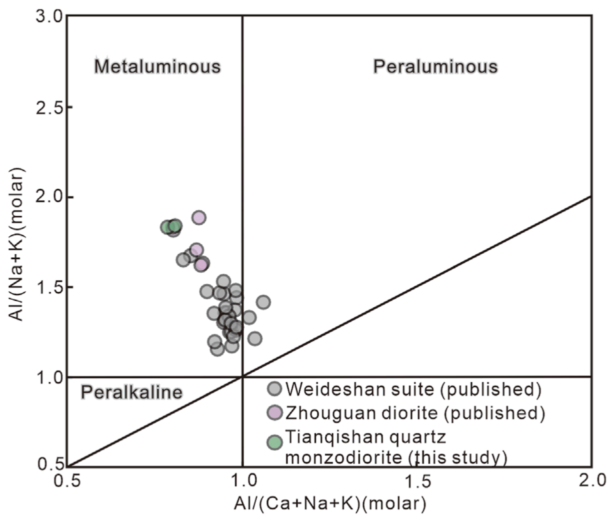

FIGURE 5
A/NK [molar ratio $Al_2O_3/(Na_2O + K_2O)$] vs. A/CNK [molar ratio $Al_2O_3/(CaO + Na_2O + K_2O)$] plot of the Tianqishan quartz monzodiorite and Weideshan granites, showing the subdivisions of Maniar and Piccoli (1989).

reflecting a gradual decrease in the degree of enrichment of the rock with increasing incompatibility of the elements. The trace element signature of the quartz monzodiorite reveals enrichment in large ion lithophile elements, such as strontium (Sr), a weak positive anomaly for barium (Ba), and significant depletion of high field strength elements, such as niobium (Nb) (Figure 7b).

4.2 Zircon U–Pb isotopes

In the present study, zircons from the Tianqishan quartz monzodiorite exhibit pronounced oscillatory zoning, which is characteristic of magmatic zircons (Figure 8a). Seventeen zircon grains from sample SQ01 were subjected to laser ablation–inductively coupled plasma-mass spectrometry (LA-ICP-MS) analysis. The Th/U ratios of these zircons range from 1.24 to 1.84, which is also indicative of a magmatic origin.

The results, as detailed in Supplementary Table S2, show that the $^{206}Pb/^{238}U$ ages of the 17 analyzed spots are clustered between 116 ± 3 Ma (1σ) and 120 ± 4 Ma (1σ). On the $^{206}Pb/2^{38}U$ concordia plot, all the spots are projected either on or close to the concordia curve, reflecting their high concordance (Figure 8b). The weighted mean $^{206}Pb/^{238}U$ age is calculated to be 119 ± 1 Ma (1σ) (Figure 8c). No ancient inherited zircons were observed in the sample.

4.3 Zircon *in situ* Hf isotopes

The results from *in situ* Hf isotopes analyses of zircons are listed in Supplementary Table S3 and shown in Figure 9. The $^{176}Lu/^{177}Hf$ ratios of all the tested zircon points range from 0.000545 to 0.001551, which are all less than 0.002, indicating that the degree of accumulation of radiogenic Hf in zirzon is low after its formation; thus the Hf isotopic composition of zircon can be used to explore rock genesis.

Seventeen zircons from sample SQ01 have initial $^{176}Hf/^{177}Hf$ values between 0.282125 and 0.282235, with an average value of 0.282178. The εHf(t) values range from −20.3 to −16.3, with an average value of −18.4. The T_{DM2} ages range from 2,200 to 2,443 Ma, with an average value of 2,325 Ma.

4.4 Apatite fission tracks

In this study, AFT analysis was conducted on one sample (SQ01) from the Tianqishan quartz monzodiorite, which yields 31 single-grain AFT ages and 64 confined track lengths. The results can be found in Supplementary Table S4, Figures 10a,b. Sample SQ01 passes the P (χ^2) test, with a value of 60%, indicating that the single-grain AFT ages in this analysis originated from the same age population. The pooled age of the sample is 112.6 ± 6.0 Ma (1σ), and the central age is 118.1 ± 5 Ma (1σ) (Figure 10a). The mean confined track length is 13.46 ± 1.86 μm (1σ), with diameter parameter (Dpar) values ranging from 1.83 to 2.93 and an average of 2.23. The track length distribution is unimodal and negatively skewed, suggesting that the pluton experienced a single cooling history. Notably, some track lengths are relatively short, implying that the sample resided in the partial annealing zone (PAZ) for an extended period (Figure 10b).

4.5 Thermal modeling

Using Hefty software (version 1.9.3), we applied the polythermal annealing kinetics model of Ketcham (2005) and the Monte Carlo approximation technique to simulate the thermal history of the AFT. The initial fission track length was set at 16.3 μm, with a surface temperature of 20°C ± 5°C and an elevation at 194 m.

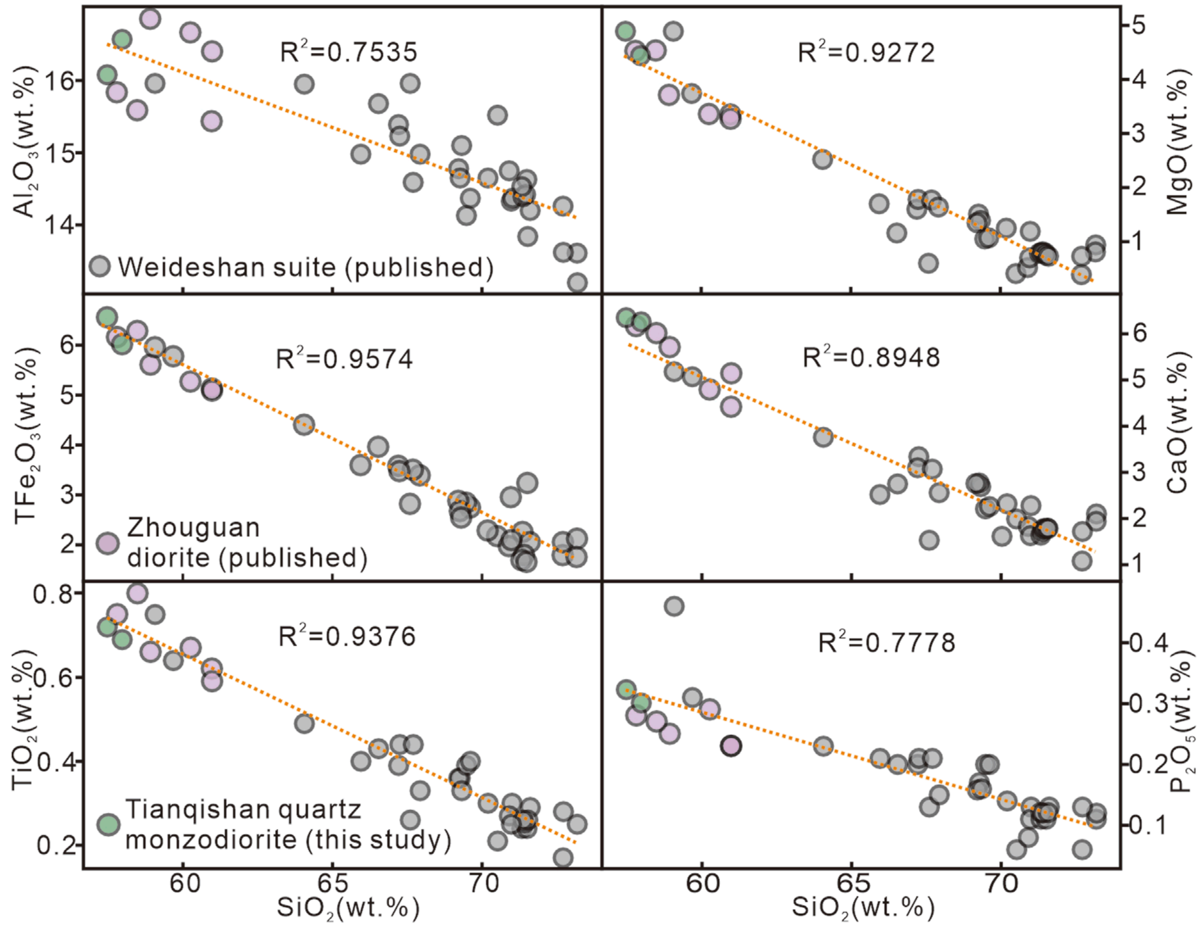

FIGURE 6
Major element Harker diagrams of the Tianqishan quartz monzodiorite and Weideshan granites.

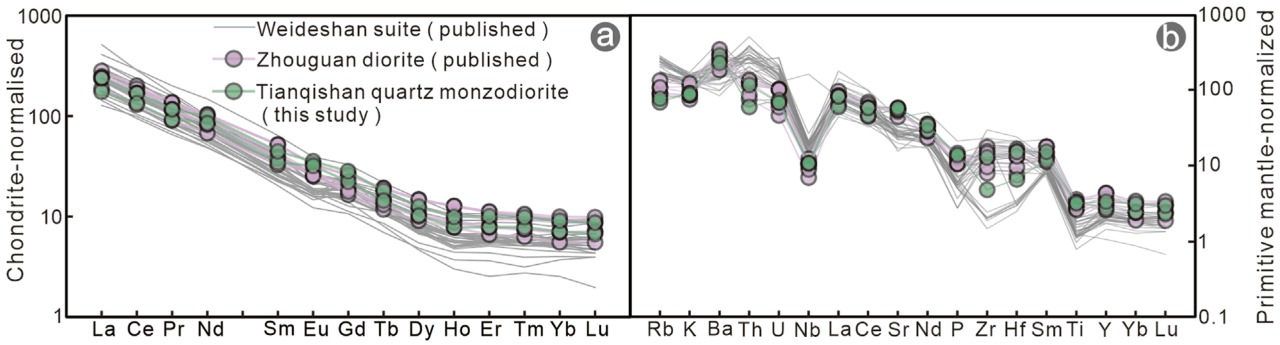

FIGURE 7
(a) Chondrite-normalized REE patterns and **(b)** primitive mantle-normalized trace element spidergrams for the later Early Cretaceous granites in the Jiaodong Peninsula. The chondrite REE and primitive mantle values were normalized after Sun and McDonough (1989).

Two time-temperature boundary conditions were established. First, the zircon U-Pb age of the sample (119 ± 1 Ma) overlaps with the AFT pooled age (112.6 ± 6.0 Ma) within the error range. Considering that the cooling of a small volume of intrusive magma to the solidus line may take only a few thousand years (Annen, 2011; Ma and Li, 2017), the fission track results for this sample may indicate both the cooling of the magma and the exhumation process (Cao et al., 2019). Therefore, the first time-temperature constraint was set at 150°C ± 10°C and 124–113 Ma, where the former delimits the thermal equilibrium process, and the latter represents the extreme values within the error range of the single-grain zircon age, together constraining the postemplacement cooling process of the magma. The second constraint was set at 90°C ± 30°C and 112.6 ± 6.0 Ma, which was

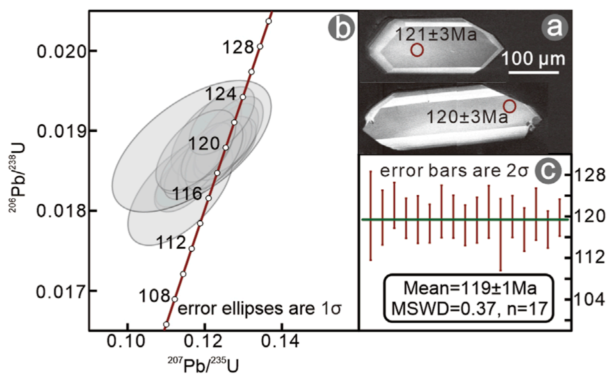

FIGURE 8
(a) Representative CL images of internal grains, **(b)** concordia diagrams and **(c)** $^{206}Pb/^{238}U$ weighted mean ages of zircons in the Tianqishan quartz monzodiorite analyzed via LA-ICP-MS.

based on the temperature range of the partial annealing zone of apatite and the pooled age, respectively.

The simulation was terminated after 500 "good" results were achieved to ensure statistical significance. The simulated ages and fission track lengths closely matched the actual measurements, with goodness-of-fit (GOF) values of 0.97 and 0.93, respectively, indicating a high degree of reliability in the simulation outcomes (Figure 11a).

The simulation results indicate that the Tianqishan quartz monzodiorite experienced four stages of cooling (Figure 11a):

1. An extremely rapid cooling period occurred from 124 Ma to approximately 120 Ma. It may indicate crustal uplift and cooling processed, as well as thermal equilibrium with the magma and country rocks. From 123 to 120 Ma, the cooling rate gradually decreased.
2. A relatively slow cooling period occurred from 120 Ma to 108 Ma. During this time, the temperature decreased by 18°C, with a cooling rate of approximately 1.5°C/Ma. According to the geothermal gradient of 44°C/km during the Early Cretaceous (Tang, 1998), the uplift was approximately 400 m.
3. A tectonic tranquility period ranged from 108 Ma to 65 Ma. During this time, the exposure of the Tianqishan quartz monzodiorite almost ceased.
4. A rapid cooling period occurred from 65 Ma to 58 Ma. During this time, the temperature of the Tianqishan quartz monzodiorite decreased by approximately 49°C, with a cooling rate of approximately 7°C/Ma. In this stage, it was uplifted over 1,100 m to a position near the Earth's surface.

5 Discussions

5.1 Geochronology, magmatic source and petrogenesis of the Tianqishan quartz monzodiorite

In this study, the newly discovered Tianqishan quartz monzodiorite was selected for zircon U–Pb isotope dating, which yields an age of 119 ± 1 Ma with good concordance. This age is younger than that of the surrounding Linglong granites (164 Ma–140 Ma) and slightly younger than the Guojialing granites (135 Ma–125 Ma) (Song et al., 2022). It emplaced almost simultaneously with the Zhouguan (118 Ma–119 Ma) (Wang et al., 2024b), Nansu (121 Ma) (Hu, 2019), Gushan (120 Ma) (Li et al., 2012), Yuangezhuang (120 Ma) (Ni et al., 2025), and Liulinzhuang (122 Ma – 118 Ma) (Song et al., 2020a) plutons. Meanwhile, it is slightly older than the Aishan (115 Ma – 116 Ma) (Hu, 2019; Li et al., 2022; Liu et al., 2025) plutons. Therefore, the Tianqishan quartz monzodiorite is the representative of the early stage of Weideshan suite (Wang et al., 2024a).

According to the characteristics of high MgO concentration (4.44 wt%–4.89 wt%) and high Mg# values (59.42–59.69), the Tianqishan quartz monzodiorite could be defined as high-Mg diorite (Chen et al., 2013). At the same time, the Tianqishan quartz monzodiorite has high Sr concentration ($1{,}164 \times 10^{-6}$–$1{,}232 \times 10^{-6}$) and low Y concentration (12.5×10^{-6}–15.3×10^{-6}). Its $(La/Yb)_N$ and Sr/Y ratios are (23.07–24.74 and 80.52–93.12, respectively) (Figures 12a,b). Therefore, the Tianqishan quartz monzodiorite has similar geochemical characteristics to high-Mg adakite (Martin et al., 2005; Moyen, 2009) and these two share a comparable origin (Kamei et al., 2004; Yin et al., 2010; Song et al., 2020a), indicating that its primary magma is ralated to mantle (Xu et al., 2002; Gao et al., 2004; Martin et al., 2005; Chen et al., 2013). This is also evidenced by the relatively high Cr (77.8×10^{-6}–78.1×10^{-6}), Ni (21×10^{-6}–22.8×10^{-6}), Co. (15.4×10^{-6}–16.5×10^{-6}) and Sc (11.7×10^{-6}–17.9×10^{-6}) concentrations and the obvious depletion of Zr concentration (54×10^{-6} -144×10^{-6}) of the Tianqishan quartz monzodiorite (Rapp and Watson, 1995). In the Na_2O vs K_2O diagram, the samples plot in the I-type granite area (Figure 12c), suggesting that the Tianqishan quartz monzodiorite is the product of the mixing of crust-derived magma and mantle-derived magma. In the Yb + Ta vs. Rb diagram, the samples all plot in the volcanic arc granite (VAG) category (Figure 12d).

Moreover, the zircon $\varepsilon_{Hf}(t)$ values range from −20.3 to −16.3, with an average value of −18.4. In the $\varepsilon_{Hf}(t)$ vs age diagram, the Tianqishan quartz monzodiorite is located between the crustal evolution lines at 2,000 Ma and 2,500 Ma, which is consistent with other Weideshan suites (Li et al., 2012; Li et al., 2022). The T_{DM2} ages, with an average value of 2,325 Ma, are consistent with the age of the Precambrian metamorphic basement of the Jiaobei Terrane, indicating that the Precambrian metamorphic basement was the main magma source.

Therefore, based on the comprehensive analysis of geochemical characteristics and zircon Lu-Hf isotopes signatures, the Tianqishan quartz monzodiorite is interpreted as having a mixed mantle and crustal origin, with its magma sourced primarily from the remelting of ancient crustal materials, that is consistent with the Zhouguan diorite and other Weideshan suites which have similar geochemical characteristics and emplacement ages (Song et al., 2020b; Wang et al., 2024b). The crystallisation ages and geochemical data jointly constrain that the Tianqishan quartz monzodiorite formed in an extensional setting induced by Paleo–Pacific plate subduction retreat and the thinning of the North China lithosphere.

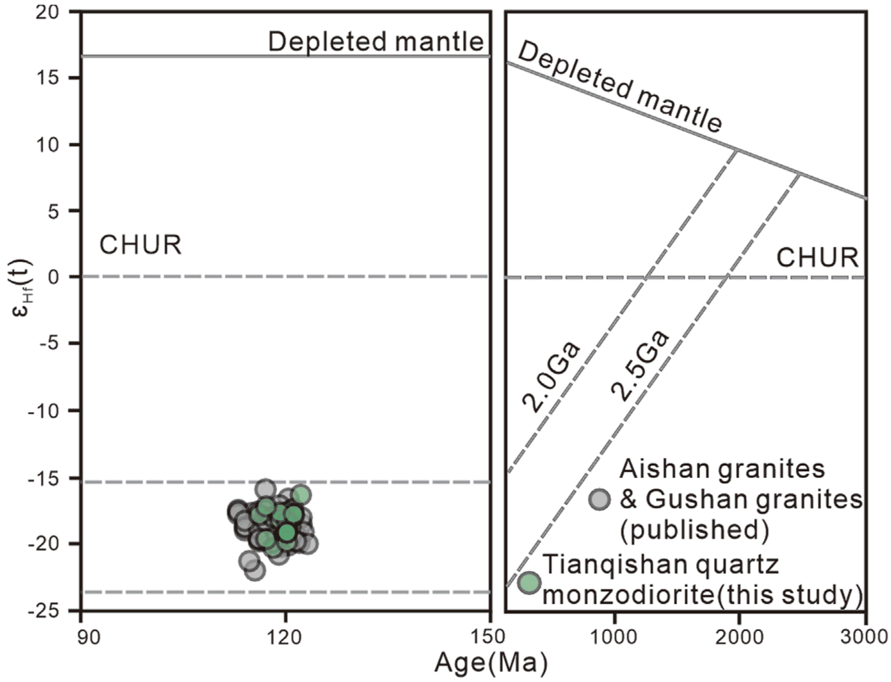

FIGURE 9
Plots of the zircon εHf(t) values vs ages of the Tianqishan quartz monzodiorite rocks. The data for Aishan granites and Gushan granites were obtained from Li et al. (2022) and Li et al. (2012). CHUR, chondrite uniform reservoir.

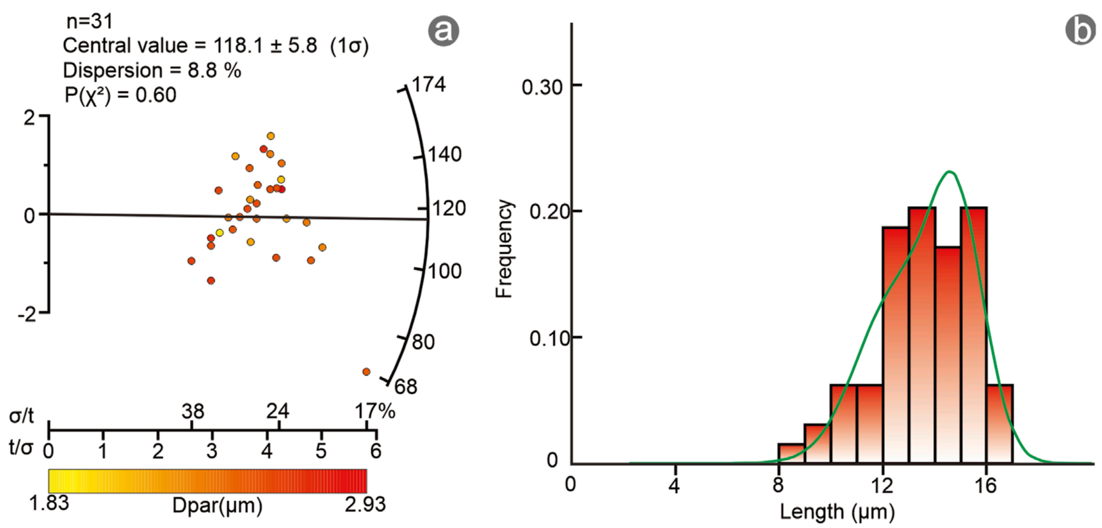

FIGURE 10
(a) Radial plots for AFT ages. Dpar: diameter parameter; P (χ2): chi-square Test; σ/t: relative error of the data; t/σ: the accuracy of the data; **(b)** histograms of the AFT length distributions (the green line represents the modeled distributions mentioned below).

5.2 The relationships between the Tianqishan quartz monzodiorite and gold mineralization

The emplacement age (119 ± 1 Ma) is remarkable consistent with that of the Zhouguan high-Mg diorites. Significantly, it represents the closest temporal association with gold mineralization events among all the intrusive rocks in the region, second only to the mafic dikes in the northwestern Jiaobei Terrane (Deng et al., 2020; Wang et al., 2024a). These chronological relationships strongly suggest that both the Tianqishan quartz monzodiorite and the Zhouguan high-Mg diorites were emplaced during the critical metallogenic epoch, potentially representing synmineralization magmatic products associated with gold-forming

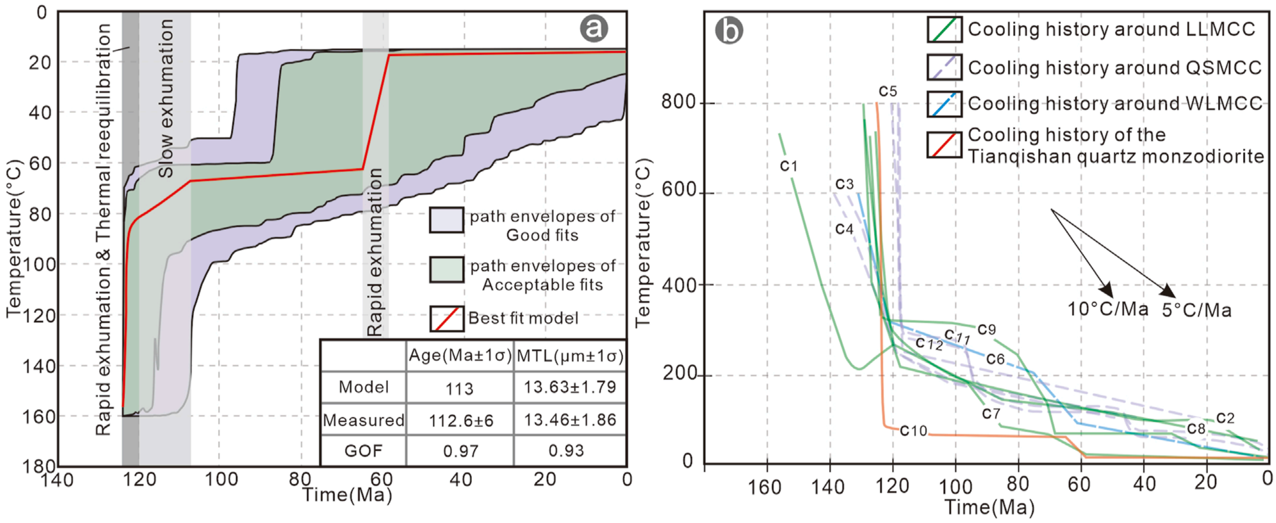

FIGURE 11
(a) Simulated thermal history of the Tianqishan quartz monzodiorite. MTL is the mean track length; σ is the standard deviation; GOF is the goodness of fit (statistical comparison of the measured input data and modeled output data, where a "good" result corresponds to a value of 0.5 or greater and "the best" result corresponds to a value of 1); a "good" result corresponds to a value of 0.50 or greater, which is the expected value if the time-temperature path and kinetic model are correct. An "acceptable" result corresponds to a value of 0.05 or higher; these values indicate that the model has not failed the null hypothesis test that forms the basis of these statistics. The dark gray area represents rapid exhumation with thermal reequilibration, and the light gray area represents rapid exhumation. **(b)** Cooling histories of different geological bodies in Jiaodong Peninsula since the Early Cretaceous. c1 and c2: Linglong pluton and Guojialing pluton, respectively in Xiadian gold deposit (Yang et al., 2023), c3, c4 and c5: Queshan pluton around Queshan metamorphic core complex (QSMCC), ductile shear zone of QSMCC and Yuangezhuang pluton around QSMCC, respectively (Ni et al., 2025), c6: Wulian metamorphic core complex (Ni et al., 2016), c7: Jiaojia gold deposit (Sun et al., 2022), c8: Guojialing pluton in Xincheng gold deposit (Zhang et al., 2019), c9: Guojialing pluton in Xinli gold deposit (Zhang et al., 2017), c10: Tianqishan quartz monzodiorite, this study. c11 and c12: Yuangezhuang and Yashan pluton, Respectively around QSMCC (Wu et al., 2018).

processes. Nevertheless, to date, no gold mineralization clues related to the intrusive rocks formed during this period have been identified in their vicinity.

The Weideshan suites intruded at shallow crustal levels (≤5 km) (Dou et al., 2015), whereas Jiaodong gold deposits developed at greater depths of 5–10 km (Song et al., 2022). This may be the reason why no gold ores are found in the Weideshan suites. The deep-seated portions of the Weideshan-type granite may represent favorable environments for mineralization.

5.3 Thermal history of the Jiaodong Peninsula since the early cretaceous

During the Early Cretaceous, the Jiaodong Peninsula experienced intense extension driven by rollback of the Paleo-Pacific Plate, leading to the formation of a series of extensional structures represented by MCCs such as Linglong (Wu and Zhu, 2024), Queshan (Ni et al., 2025), and Wulian (Ni et al., 2013; Ni et al., 2016). Numerous studies have proposed that the large-scale gold mineralization in this region is genetically linked to this extensional regime (Song et al., 2018; Wang et al., 2023). The Tianqishan quartz monzodiorite, intruded into the core of the Linglong MCC, reveals that its emplacement timing closely coincides with the Yashan and Yanggezhuang plutons (Ni et al., 2025) adjacent to the Queshan MCC, while the Guojialing pluton (Yang et al., 2023) shows slightly earlier emplacement. These plutons share remarkably similar post-emplacement cooling histories (Figure 11b), characterized by steep time-temperature curves that significantly exceed the contemporaneous cooling rates of both the Jiaodong MCCs and earlier emplaced plutons (e.g., Linglong and Queshan granitoids) (Yang et al., 2023; Ni et al., 2025). Considering the probable syn-emplacement uplift of the Tianqishan quartz monzodiorite and other coeval plutons, coupled with the abrupt onset of rapid cooling immediately following their emplacement, we propose that their anomalously fast cooling rates resulted from the combined effect of regional uplift and thermal equilibration between the plutons and their country rocks. Therefore, we suggest that the moderate cooling rates (17.5°C–18.5°C/Ma) (Ni et al., 2025) recorded by large-scale extensional structures and earlier emplaced plutons (e.g., Queshan granitoid) more accurately represent the regional cooling signature of the Jiaodong Peninsula during the Early Cretaceous.

A pronounced decline in cooling rate around 120 Ma observed in the Tianqishan quartz monzodiorite (Figure 11A) shows temporal consistency with cooling histories of major gold deposits (Jiaojia, Xiadian, Xincheng, and Xinli) (Zhang et al., 2017; Zhang et al., 2019; Sun et al., 2022; Yang et al., 2023) adjacent to the Linglong MCC (Figure 11b), indicating termination of rapid exhumation of the Linglong MCC by this time. Regional correlation reveals synchronous cessation of rapid exhumation in the Queshan and Wulian MCCes (Ni et al., 2016; Ni et al., 2025), collectively suggesting substantial weakening of the extensional regime across the Jiaodong Peninsula post 120 Ma, with subsequent uplift rates decreasing to 1.5°C–3.5°C/Ma. This aligns well with the Cretaceous two-stage extensional tectonic proposed for the eastern Eurasian continent by Lin and Li (2021).

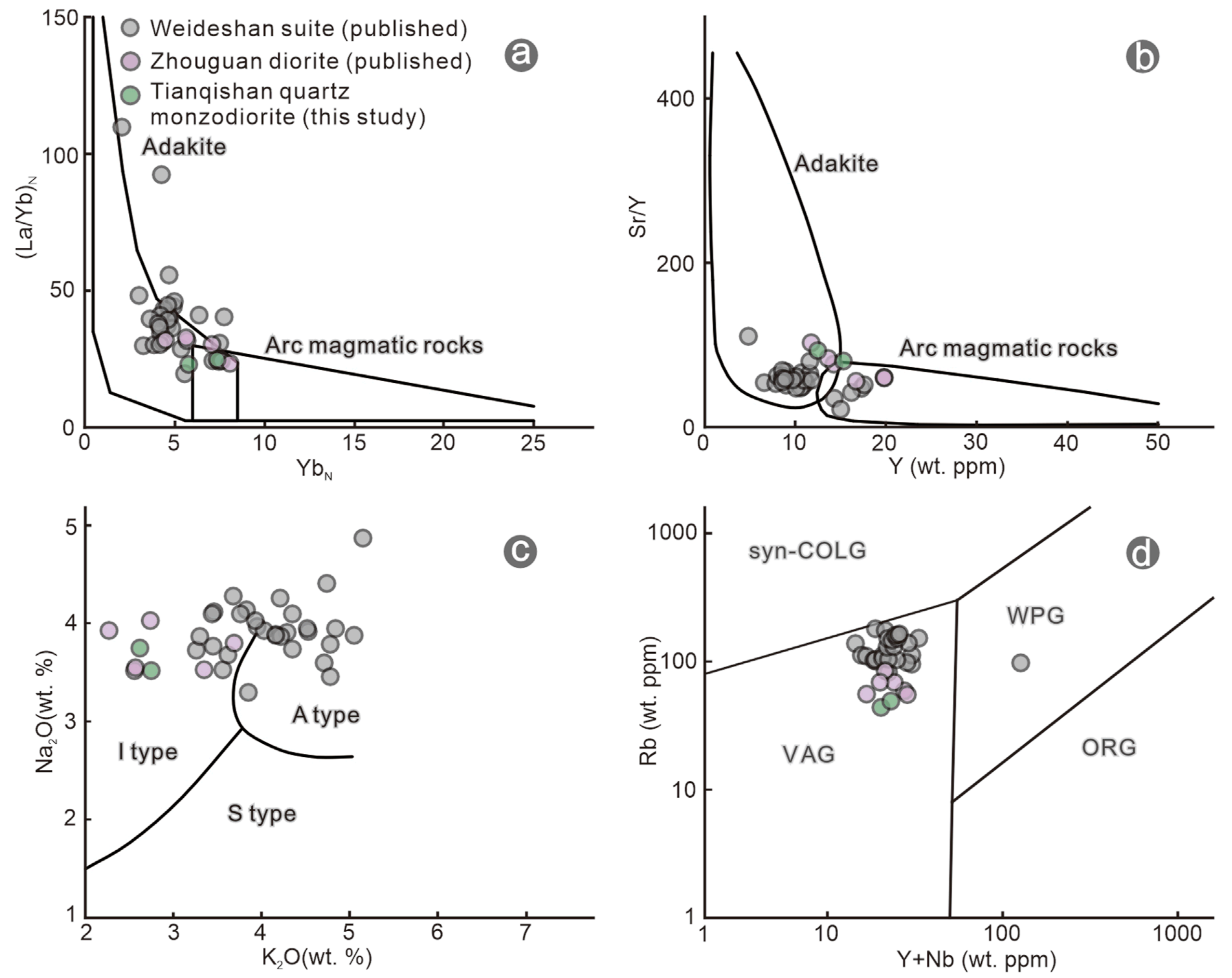

FIGURE 12
Diagrams of **(a)** Yb_N vs. $(La/Yb)_N$, **(b)** Y vs. Sr/Y, **(c)** K_2O vs. Na_2O and **(d)** Y + Nb vs. Rb for Tianqishan quartz monzodiorite in the Jiaodong Peninsula (Base map according to Martin (1986); Defant and Drummond (1990); Collins et al. (1982); Pearce et al. (1984), respectively; VAG, volcanic arc granite; Syn-COLG, syncollisional granite; WPG, within-plate granite; ORG, ocean ridge granite.).

It was noted that the Liaonan MCC in the Liaodong Peninsula and the Wulian MCC in the Jiaodong Peninsula underwent two distinct stages of tectonic-thermal evolution during the Early Cretaceous. The exhumation of the Liaonan MCC began slowly and then accelerated, whereas the Wulian MCC was initially exhumed rapidly and then decelerated (Liu et al., 2022). The Parallel Extensional Tectonics (PET) model is proposed to explain this divergence (Liu et al., 2009b; Liu et al., 2020; Liu et al., 2022). Our findings indicate that the uplift rate variations of the Linglong, Queshan, and Wulian MCCs are consistent. This consistency reflects the uniform changes in extension intensity across the entire Jiaodong Peninsula during the Early Cretaceous, suggesting the PET model's applicability to the entire region. According to the model, crustal detachment and lithospheric mantle detachment can be either coupled or decoupled. Liu et al. (2022) concluded that the significant influence of the Triassic subduction and collision between the Yangtze and North China cratons resulted in considerable lithospheric thickening, lower geothermal gradient and higher lithospheric mantle strength in the Jiaodong Peninsula compared to the Liaodong Peninsula. The lithosphere of the Jiaodong Peninsula is characterized by a strong upper crust combined with a strong lithospheric mantle, in contrast with the Liaodong Peninsula, which features a strong upper crust with a weaker lithospheric mantle. These differences in lithospheric rheological stratification led to the decoupling of the crust and mantle detachment in the Jiaodong Peninsula and coupling detachment in the Liaodong Peninsula (Liu et al., 2022). However, considering that the pre-existing structures formed in the continental collision reduced the crustal strength of the Jiaodong Peninsula, which make it more susceptible to reactivation under subsequent extensional stress fields (Tong and Yin, 2011; Tong et al., 2014b; Tong et al., 2014a; Gao et al., 2019), we argue for low crustal strength in the Jiaodong Peninsula, which contradicts Liu et al. (2022), who reported high crustal strength in the same region.

Controlled by the subduction and rollback of the ancient Pacific plate, the regional extensional tectonics of the Jiaodong Peninsula can be traced back as early as 135 million years. During this period, the relatively weak crust of the Jiaodong Peninsula underwent extensive thinning, leading to rapid exhumation of MCCs, such as the Linglong MCC and the Wulian MCC. In contrast, relatively strong lithospheric mantle has experienced only limited, localized detachment faults (Liu et al., 2022). Geochemical evidence indicates that approximately 121–122 million years ago, the juvenile subcontinental lithospheric mantle (SCLM) of the North China Craton (NCC) may have replaced the ancient SCLM, coinciding with the collapse of the lithospheric mantle and the upwelling of the asthenosphere (Dai et al., 2016; Zheng et al., 2018). The lithospheric mantle of the Jiaodong Peninsula completed its decratonization, and as regional extension continued, the destabilized lithospheric mantle began extensive thinning. Concurrently, crustal-scale extension weakened.

Different from the early Cretaceous in Jiaodong Peninsula, the thermal history of the late Cretaceous showed obvious heterogeneity, with two remarkable characteristics. Firstly, the cooling histories of different crustal domains began to diverge significantly, as evidenced by widely scattered apatite fission track (AFT) and (U-Th)/He (AHe) ages (Yang et al., 2016; Liu et al., 2017; Sun et al., 2017; Zhang et al., 2017; Li et al., 2018b; Wu et al., 2018; Zhao et al., 2018; Zhang et al., 2019; Yang et al., 2020; Zhang et al., 2020; Sun et al., 2022; Zhang et al., 2022; Qiu et al., 2023b; Yang et al., 2023; Ni et al., 2025). This observation indicates that, unlike the Early Cretaceous period dominated by the unified paleostress field associated with Paleo-Pacific Plate subduction and rollback, the Late Cretaceous tectonic regime was likely characterized by localized stress regimes controlling differential crustal behavior. Secondly, although multiple studies have documented localized episodes of relatively rapid uplift in sub-regions post-Early Cretaceous, most uplift rates remained low (<10°C/Ma), pales in comparison to the prominent Early Cretaceous rapid exhumation events. Based on these lines of evidence, we propose that the Jiaodong Peninsula transitioned into a phase of regional extension coupled with differential uplift during the Late Cretaceous.

5.4 Implications for explosive gold mineralization

The latest U–Pb dating of monazite indicates that the formation of Jiaodong Peninsula gold deposits was limited to a very narrow time range of ca. 120 ± 2 Ma (Ma et al., 2017; Li et al., 2018a; Yang et al., 2018; Deng et al., 2020), this suggests that there must have been a specific geological process, or "episodic" event, during this time that led to the explosive mineralization of gold. The subduction of the Paleo–Pacific plate plays a significant role in the tension and destruction of the North China Craton and is the primary external driving force that led to the large-scale mineralization of gold in Jiaodong (Xu, 2001; Zhang et al., 2009; Zheng and Wu, 2009; Zhu and Zheng, 2009; Wu et al., 2014; Deng et al., 2022; Song et al., 2022; Long et al., 2025a). However, it remains unclear which specific process and mechanism during subduction led to the explosive gold mineralization.

Some researchers have suggested that large-scale gold mineralization in the Jiaodong Peninsula occurred in an environment characterized by intense crustal extension and rapid uplift, which is associated with the peak destruction of the North China Craton (Song et al., 2018; Wang et al., 2023). However, the cessation of rapid crustal uplift in the region suggests that gold mineralization may have been driven by deeper geodynamic processes.

The subduction direction of the Paleo–Pacific plate changed at ca. 122 Ma (Ni et al., 2024), while a high rate of retreat of ~8.8 cm/a occurred from 130 to 120 Ma (Zhu et al., 2015). The change in the subduction direction and rate of retreat of the Paleo–Pacific plate may have led to a temporary ocean-continent collision and was associated with a temporary extrusion event on the Jiaodong Peninsula during the late Early Cretaceous, which caused an angular unconformity between the Laiyang Formation (approximately 135–125 Ma) and the Qingshan Formation (120–105 Ma) (Zhang et al., 2008; Ni et al., 2013). In addition to the eruption of the East Java plate at ca. 125 Ma (Sun and Li, 2023), the alteration of mantle convection due to the delamination of the lithospheric mantle in the Jiaodong Peninsula may have contributed to the change in the subduction direction of the Paleo–Pacific plate. Some studies believe that the change in the subduction direction of the Paleo–Pacific plate induced explosive gold mineralization in the Jiaodong Peninsula (Ni et al., 2024; Ni et al., 2025), however, further refinement is needed to fully address the mechanisms controlling the focused release of auriferous fluids.

The East Asian big mantle wedge (BMW) (Zhao, 2004; Eiji and Zhao, 2009) began to form between 145 and 140 Ma and was fully developed at approximately 120 Ma (Ma and Xu, 2021), it is closely related to the destabilization and destruction of the North China Craton (Zhu and Xu, 2019). Zhu and Sun (2021) investigated the link between the Big Mantle Wedge (BMW) and large-scale gold mineralization in the Jiaodong Peninsula, proposing that the ore-forming fluids may be derived from the stagnation of the subducting slab in the mantle transition zone. A flat-lying subducting slab within this zone can release substantial amounts of water, which facilitates the dissolution of sulfides and the extraction of gold, thereby generating gold-rich fluids. These fluids ascend through the cratonic lithospheric mantle and undergo metasomatic interaction with the surrounding mantle material (Zhu and Sun, 2021). This interaction resulted in the formation of a hydrated and gold-enriched weakened layer within the cratonic lithospheric mantle, which is necessary for explosive gold mineralization (He et al., 2024; Qiu et al., 2024a). This hypothesis has been corroborated by the latest isotope geochemical results (Wang et al., 2024b; Zhang et al., 2024). Deng et al. (2020) argued that with the continuous rollback of the ancient Pacific plate, slab-derived fluid would have been lost in the developing mantle wedge significantly prior to mineralization, and that in the Jiaodong Peninsula was attributed to the postsubduction opening of a slab gap at ca. 120 Ma; however, this speculation is difficult to prove.

In general, changes in the subduction direction and rate of retreat of the Pacific plate, final formation of the BMW, changes in the nature of the lithospheric mantle, and the gold mineralization in the Jiaodong Peninsula all occurred at ca. 120 ± 2 Ma. In fact, this period also marks the cessation of rapid crustal exhumation in the region. The temporal coincidence of these events implies a potential intrinsic linkage among them. The PET model reasonably explains the genesis of the Early Cretaceous two-stage extensional tectonics

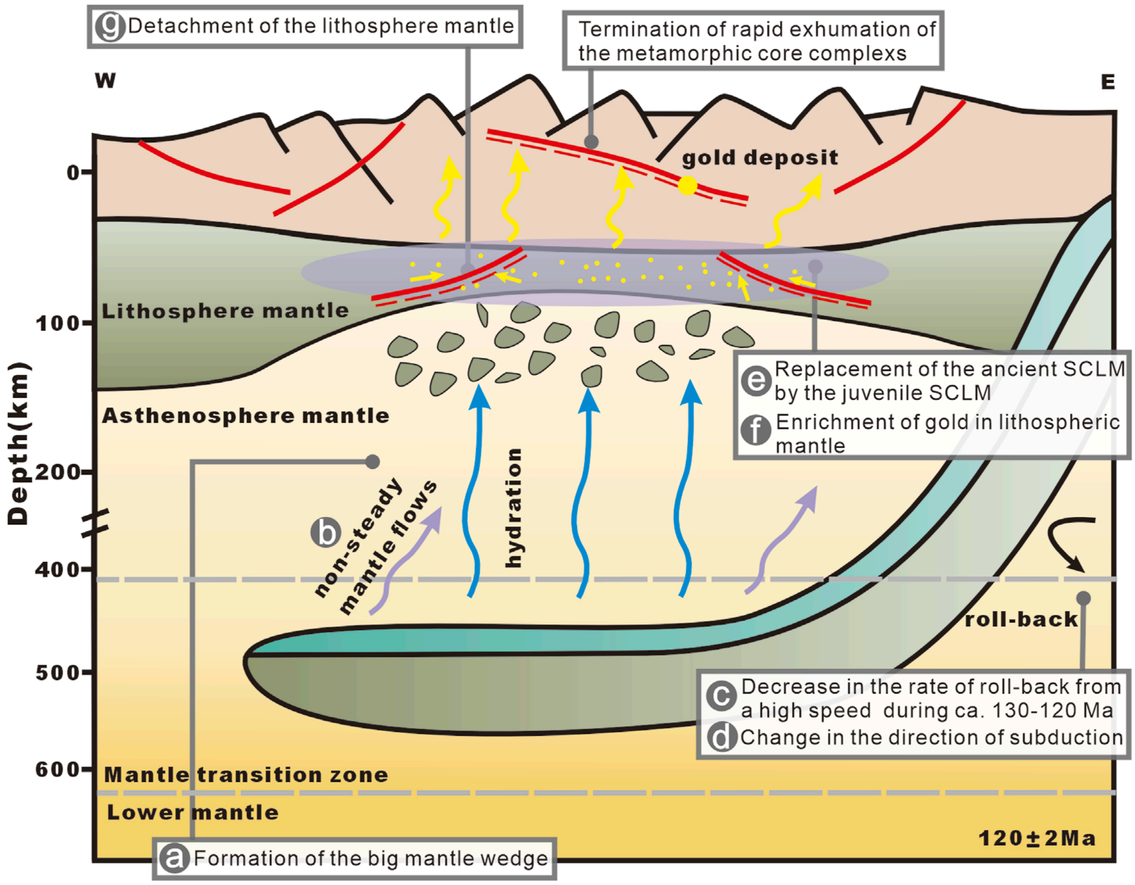

FIGURE 13
Cartoon model of the explosive gold metallogenic process at ca. 120 ± 2 Ma on the Jiaodong Peninsula. The major geological events mentioned in the cartoon can be found in the following references: (a) Ma and Xu (2021), (b) Zhu and Sun (2021), (c) Zhu and Xu (2019), (d) Ni et al. (2024), (e) Dai et al. (2016) and Zheng et al. (2018), (f) Qiu et al. (2024a), Wang X. et al. (2024b) and Zhang et al. (2024), (g) Liu et al. (2020).

in the Jiaodong Peninsula. On this basis, we propose a model of explosive gold mineralization in the Jiaodong Peninsula based on the PET model (Figure 13).

1. During the period of ~130–120 Ma, the subduction angle of the Paleo-Pacific Plate increased significantly, reaching peak rollback velocities. This phase coincided with the progressive development of a big mantle wedge, where dehydration of the subducting slab generated unstable mantle flows that facilitated metasomatic enrichment of gold within the lithospheric mantle. Due to the strength contrast between crust and mantle, decoupling occurred during lithospheric extension: the crust developed intense detachment accompanied by rapid exhumation, while the stronger lithospheric mantle localized detachment faulting only in discrete zones. This decoupling effectively preserved gold reservoirs within the mantle lithosphere, establishing the essential endowment for subsequent explosive gold mineralization.
2. At approximately 120 ± 2 Ma, the lithospheric mantle beneath the Jiaodong Peninsula underwent complete decratonization. This process resulted in the loss of mechanical strength in the previously rigid cratonic lithospheric mantle, triggering large-scale extensional detachment that was accompanied by lithospheric root collapse and asthenospheric upwelling. Gold pre-enriched within the destabilized lithospheric mantle was channelized through these detachment zones and massively released into the crust, where pre-existing crustal extensional structures served as efficient fluid pathways and mineralization traps, facilitating ore precipitation. Concurrent deceleration of crustal uplift rates during this period likely enhanced gold deposition by prolonging fluid-rock interaction stability. Furthermore, minimal post-mineralization erosion ensured exceptional preservation of the ore systems.

6 Conclusion

1. The Tianqishan quartz monzodiorite was formed at 119 Ma, which is consistent with the large-scale gold mineralization time in the Jiaodong Peninsula. It is a metaluminous high-potassium calc-alkaline rock with geochemical characteristics of high-magnesium adakitic rock. It is a product of the partial melting of the enriched mantle and mixing with the crust in the process of magma ascent in a tectonic setting resulting from the subduction and rollback

of the Paleo–Pacific Plate and the thinning of the crust of the North China Craton.

2. The AFT thermal history modeling results reveal that the rapid exhumation of the crust of the Jiaodong Peninsula terminated at approximately 120 ± 2 Ma. This may be due to the decoupling between crustal detachment and lithospheric mantle detachment in the Jiaodong Peninsula.
3. The large-scale detachment in the "decratonized" lithospheric mantle may have been the direct factor controlling the "explosive gold mineralization" in the Jiaodong Peninsula.

Data availability statement

The original contributions presented in the study are included in the article/Supplementary Material, further inquiries can be directed to the corresponding authors.

Author contributions

JGa: Conceptualization, Methodology, Visualization, Writing – original draft, Writing – review and editing. KZ: Funding acquisition, Investigation, Project administration, Supervision, Writing – review and editing. ZD: Data curation, Investigation, Writing – review and editing. YF: Data curation, Investigation, Software, Writing – review and editing. LL: Investigation, Software, Writing – review and editing. ZW: Investigation, Writing – review and editing. JGo: Investigation, Writing – review and editing. JY: Investigation, Writing – review and editing. YL: Investigation, Writing – review and editing.

Funding

The author(s) declare that financial support was received for the research and/or publication of this article. This work was supported by the Geological Survey Project of the China Geological Survey (DD20240203702, DD20242247 and DD20230439), the Deep Earth Probe and Mineral Resources Exploration – National Science and Technology Major Project (2024ZD1003404), the Science and technology support project for the new round of strategic action to find mineral breakthroughs (ZKKJ202419), the National Key R&D Program of China (2018YFE0208300), the open fund (2022DW01) from No. 1 Institute of Geology and Mineral Resources of Shandong Province, the MOST Special Fund (GPMR202436) from the State Key Laboratory of Geological Process and Mineral Resources, China University of Geosciences, and National Nonprofit Institute Research Grant (AS2020Y05, AS2024J13 and AS2022J11)

Acknowledgments

We gratefully acknowledge the Handling Editor Kunfeng Qiu and two reviewers for their valuable comments.

Conflict of interest

The authors declare that the research was conducted in the absence of any commercial or financial relationships that could be construed as a potential conflict of interest.

The reviewer PC declared a shared affiliation with the authors to the handling editor at time of review.

Generative AI statement

The author(s) declare that no Generative AI was used in the creation of this manuscript.

Publisher's note

All claims expressed in this article are solely those of the authors and do not necessarily represent those of their affiliated organizations, or those of the publisher, the editors and the reviewers. Any product that may be evaluated in this article, or claim that may be made by its manufacturer, is not guaranteed or endorsed by the publisher.

Supplementary material

The Supplementary Material for this article can be found online at: https://www.frontiersin.org/articles/10.3389/feart.2025.1572864/full#supplementary-material

References

Annen, C. (2011). Implications of incremental emplacement of magma bodies for magma differentiation, thermal aureole dimensions and plutonism–volcanism relationships. *Tectonophysics* 500, 3–10. doi:10.1016/j.tecto.2009.04.010

Cao, K., Wang, G., Leloup, P. H., Mahéo, G., Xu, Y., van der Beek, P. A., et al. (2019). Oligocene-early miocene topographic relief generation of southeastern tibet triggered by thrusting. *Tectonics* 38, 374–391. doi:10.1029/2017TC004832

Chai, P., Hou, Z., Zhang, H., and Dong, L. (2019a). Geology, fluid inclusion, and H–O–S–Pb isotope constraints on the mineralization of the xiejiagou gold deposit in the Jiaodong Peninsula. *Geofluids* 2019, 1–23. doi:10.1155/2019/3726465

Chai, P., Hou, Z., and Zhang, Z. (2017). Geology, fluid inclusion and stable isotope constraints on the fluid evolution and resource potential of the xiadian gold deposit, Jiaodong Peninsula. *Resour. Geol.* 67, 341–359. doi:10.1111/rge.12134

Chai, P., Zhang, H., Dong, L., and Zhang, Z. (2019b). Geology and ore-forming fluids of the Dayingezhuang gold deposit, Jiaodong Peninsula, eastern China: implications for mineral exploration. *J. Geochem. Explor.* 204, 224–239. doi:10.1016/j.gexplo.2019.06.001

Chai, P., Zhang, H., Hou, Z., and Zhang, Z. (2020a). Geochronological framework of the Damoqujia gold deposit, Jiaodong Peninsula, China: implications for the timing and geologic setting of gold mineralization. *Geol. J.* 55, 596–613. doi:10.1002/gj.3428

Chai, P., Zhang, H., Hou, Z., Zhang, Z., and Dong, L. (2020b). Ore geology, fluid inclusion, and stable isotope constraints on the origin of the Damoqujia gold deposit, Jiaodong Peninsula, China. *Can. J. Earth Sci.* 57, 1428–1446. doi:10.1139/cjes-2018-0247

Chai, P., Zhang, Z., and Hou, Z. (2019c). Geological and fluid inclusion constraints on gold deposition processes of the dayingezhuang gold deposit, Jiaodong Peninsula, China. *Acta Geol. Sin. Eng.* 93, 955–971. doi:10.1111/1755-6724.13849

Charles, N., Augier, R., Gumiaux, C., Monié, P., Chen, Y., Faure, M., et al. (2013). Timing, duration and role of magmatism in wide rift systems: insights from the Jiaodong Peninsula (China, East Asia). *Gondwana Res.* 24, 412–428. doi:10.1016/j.gr.2012.10.011

Charles, N., Chen, Y., Augier, R., Gumiaux, C., Lin, W., Faure, M., et al. (2011). Palaeomagnetic constraints from granodioritic plutons (Jiaodong Peninsula): new insights on late mesozoic continental extension in eastern asia. *Phys. Earth Planet. Interiors* 187, 276–291. doi:10.1016/j.pepi.2011.05.006

Chen, B., Jahn, B.-M., and Suzuki, K. (2013). Petrological and Nd-Sr-Os isotopic constraints on the origin of high-Mg adakitic rocks from the North China Craton: tectonic implications. *Geology* 41, 91–94. doi:10.1130/G33472.1

Chen, Y., Li, H., Gu, S., Whattam, S. A., Zheng, C., Wang, L., et al. (2025). Geochemistry, geochronology and Fe-Mg-S isotopic composition of the Liaoshang gold deposit, Jiaodong Peninsula, China: implications for ore-forming processes and mineral exploration. *J. Geochem. Explor.* 273, 107738. doi:10.1016/j.gexplo.2025.107738

Collins, W. J., Beams, S. D., White, A. J. R., and Chappell, B. W. (1982). Nature and origin of A-type granites with particular reference to southeastern Australia. *Contrib. Mineral. Petrol* 80, 189–200. doi:10.1007/BF00374895

Cui, T., Yu, H., Jowitt, S., Li, Z., Wei, X., and Zou, S. (2025). Chlorite composition reflecting increased oxygen fugacity-induced disseminated mineralization in the Guocheng gold deposit, China. *GSA Bull.* doi:10.1130/B38151.1

Dai, L., Zheng, Y., and Zhao, Z. (2016). Termination time of peak decratonization in North China: geochemical evidence from mafic igneous rocks. *Lithos* 240-243, 327–336. doi:10.1016/j.lithos.2015.11.014

Defant, M. J., and Drummond, M. S. (1990). Derivation of some modern arc magmas by melting of young subducted lithosphere. *Nature* 347, 662–665. doi:10.1038/347662a0

Deng, J., Liu, X., Wang, Q., and Pan, R. (2015). Origin of the Jiaodong-type Xinli gold deposit, Jiaodong Peninsula, China: constraints from fluid inclusion and C–D–O–S–Sr isotope compositions. *Ore Geol. Rev.* 65, 674–686. doi:10.1016/j.oregeorev.2014.04.018

Deng, J., Qiu, K., Wang, Q., Goldfarb, R., Yang, L., Zi, J., et al. (2020). Insitu dating of hydrothermal monazite and implications for the geodynamic controls on ore formation in the Jiaodong gold province, eastern China. *Econ. Geol.* 115, 671–685. doi:10.5382/econgeo.4711

Deng, J., Wang, Q., Liu, X., Zhang, L., Yang, L., Yang, L., et al. (2022). The Formation of the Jiaodong gold province. *Acta Geol. Sin. Eng.* 96, 1801–1820. doi:10.1111/1755-6724.15026

Dou, J., Fu, S., and Zhang, H. (2015). Consolidation and cooling paths of the Guojialing granodiorites in Jiaodong Peninsula: implication for crustal uplift and exhumation. *Acta Petrol. Sin.* 31, 2325–2336.

Du, B., Deng, J., Santosh, M., Wang, Z., Shen, Y., Liu, S., et al. (2025). Role of impurities in the semiconducting properties of natural pyrite: implications for the electrochemical accumulation of visible gold and formation of hydrothermal gold deposits. *Am. Mineralogist* 110, 189–216. doi:10.2138/am-2023-9187

Eiji, O., and Zhao, D. (2009). The role of water in the deep upper mantle and transition zone: dehydration of stagnant slabs and its effects on the big mantle wedge. *Russ. Geol. Geophys.* 50, 1073–1078. doi:10.1016/j.rgg.2009.11.006

Fan, H. R., Zhai, M. G., Xie, Y. H., and Yang, J. H. (2003). Ore-forming fluids associated with granite-hosted gold mineralization at the Sanshandao deposit, Jiaodong gold province, China. *Miner. Deposita* 38, 739–750. doi:10.1007/s00126-003-0368-x

Fang, Y., Liang, Y., Xia, R., Shu, L., He, B., Xue, W., et al. (2025). Geochemistry of pyrite from the Jiaojia gold deposit, Jiaodong Peninsula, north China craton: implications for source of ore-forming fluids and gold precipitation. *Appl. Sci.* 15, 1548. doi:10.3390/app15031548

Feng, Y., Qiu, K., Wang, D., Sha, W., and Li, S. (2022). Forming conditions of tellurides and their constraints on gold enrichment in Linglong gold district, Jiaodong gold province. *Acta Geol. Sin.* 38, 63–77. doi:10.18654/1000-0569/2022.01.05

Gao, B., and Li, Z. (2020). Differential exhumation of Jiaodong Peninsula during early cretaceous: evidence from detrital zircon U–Pb isotopic dating. *Geol. J.* 55, 2773–2786. doi:10.1002/gj.3541

Gao, J., Lin, Y., Zhang, C., Ding, Z., Hou, L., and Huang, Y. (2019). Late mesozoic paleotectonic stress fields inferred from fault-slip data in central and western yanshan orogenic belt: implications for destructive geodynamics of North China craton. *Geoscience* 33, 919–936. doi:10.19657/j.geoscience.1000-8527.2019.05.01

Gao, S., Rudnick, R. L., Yuan, H., Liu, X., Liu, Y., Xu, W., et al. (2004). Recycling lower continental crust in the North China craton. *Nature* 432, 892–897. doi:10.1038/nature03162

Geng, J., Li, H., Zhang, J., Zhou, H., and Li, H. (2011). Zircon Hf isotope analysis by means of LA-MC-ICP-MS. *Geol. Bull. China* 30, 1508–1513.

Goldfarb, R. J., and Santosh, M. (2014). The dilemma of the Jiaodong gold deposits: are they unique? *Geosci. Front.* 5, 139–153. doi:10.1016/j.gsf.2013.11.001

Hacker, B. R., Wallis, S. R., Mcwilliams, M. O., and Gans, P. B. (2009). 40 Ar/39 Ar Constraints on the tectonic history and architecture of the ultrahigh-pressure Sulu orogen. *J. Metamorph. Geol.* 27, 827–844. doi:10.1111/j.1525-1314.2009.00840.x

Hasebe, N., Barbarand, J., Jarvis, K., Carter, A., and Hurford, A. J. (2004). Apatite fission-track chronometry using laser ablation ICP-MS. *Chem. Geol.* 207, 135–145. doi:10.1016/j.chemgeo.2004.01.007

He, D., Qiu, K., Simon, A. C., Pokrovski, G. S., Yu, H., Connolly, J. A. D., et al. (2024). Mantle oxidation by sulfur drives the formation of giant gold deposits in subduction zones. *Proc. Natl. Acad. Sci. U.S.A.* 121, e2404731121. doi:10.1073/pnas.2404731121

Hu, B. (2019). Chronology, geochemical characteristics and tectonic significance of the aishan—nansu pluton in Jiaodong. *Master*. doi:10.27752/d.cnki.gsjzj.2019.000206

Hu, Z., Liu, Y., Gao, S., Liu, W., Zhang, W., Tong, X., et al. (2012). Improved *in situ* Hf isotope ratio analysis of zircon using newly designed X skimmer cone and jet sample cone in combination with the addition of nitrogen by laser ablation multiple collector ICP-MS. *J. Anal. Atomic Spectrom.* 27, 1391–1399. doi:10.1039/C2JA30078H

Kamei, A., Owada, M., Nagao, T., and Shiraki, K. (2004). High-Mg diorites derived from sanukitic HMA magmas, Kyushu Island, southwest Japan arc: evidence from clinopyroxene and whole rock compositions. *Lithos* 75, 359–371. doi:10.1016/j.lithos.2004.03.006

Ketcham, R. A. (2005). Forward and inverse modeling of low-temperature thermochronometry data. *Rev. Mineralogy Geochem.* 58, 275–314. doi:10.2138/rmg.2005.58.11

Kuang, H., Yan, J., Zhang, K., Tang, W., Fu, C., Liang, J., et al. (2025). Integrated geophysical signatures of the Jiaodong region in China and their implications for deep architecture and gold metallogenic systems. *Minerals* 15, 417. doi:10.3390/min15040417

Le Maitre, R.W. (1989). A classification of igneous rocks and glossary of terms. in: *Recommendations of the international union of geological sciences subcommission on the systematics of igneous rocks*. Oxford: Blackwell Scientific Publications. 193.

Li, H., Lu, S., Li, H., Sun, L., Xiang, Z., Geng, J., et al. (2009). Zircon and beddeleyite U-Pb precision dating of basic rock sills intruding Xiamaling Formation, North China. *Geol. Bull. China* 28, 1396–1404.

Li, J., Zhang, L., Song, M., Wang, J., Yan, M., and Sun, W. (2025). Destruction of the North China craton account for the shijia gold deposit in the Jiaodong Peninsula, eastern China. *Ore Geol. Rev.* 181, 106609. doi:10.1016/j.oregeorev.2025.106609

Li, X., Fan, H., Santosh, M., Hu, F., Yang, K., Lan, T., et al. (2012). An evolving magma chamber within extending lithosphere: an integrated geochemical, isotopic and zircon U–Pb geochronological study of the Gushan granite, eastern North China Craton. *J. Asian Earth Sci.* 50, 27–43. doi:10.1016/j.jseaes.2012.01.016

Li, X., Fan, H., Yang, K., Hollings, P., Liu, X., Hu, F., et al. (2018a). Pyrite textures and compositions from the Zhuangzi Au deposit, southeastern North China Craton: implication for ore-forming processes. *Contrib. Mineral. Petrol* 173, 73. doi:10.1007/s00410-018-1501-2

Li, X., Fan, H., Zhang, Y., Hu, F., Yang, K., Liu, X., et al. (2018b). Rapid exhumation of the northern Jiaobei Terrane, north China craton in the early cretaceous: insights from Al-in-hornblende barometry and U-Pb geochronology. *J. Asian Earth Sci.* 160, 365–379. doi:10.1016/j.jseaes.2017.10.001

Li, X., Wang, L., Li, Y., Wang, Y., Yu, X., Zhang, W., et al. (2022). Zircon U-Pb chronology and Lu-Hf isotope characteristics of monzogranites from aishan pluton in Jiaodong Peninsula. *Geoscience* 36, 333–346. doi:10.19657/j.geoscience.1000-8527.2022.01.30

Lin, W., and Li, J. (2021). Cretaceous two stage extensional tectonic in eastern Eurasia continent and its geodynamics. *Acta Petrol. Sin.* 37, 2303–2323. doi:10.18654/1000-0569/2021.08.04

Liu, J., Ji, L., Ni, J., and Chen, X. (2022). Dynamics of the Early Cretaceous lithospheric thinning and destruction of the North China craton as the consequence of Paleo-Pacific type active continental margin. *Acta Geol. Sin.* 96, 3360–3380. doi:10.19762/j.cnki.dizhixuebao.2022178

Liu, J., Ji, M., Xia, H., Liu, Z., Zhou, Y., Yu, X., et al. (2009a). Crustal-mantle detachment of the North China craton in late mesozoic: rheological constraints. *Acta Petrol. Sin.* 25, 1819–1829.

Liu, J., Ni, J., Chen, X., Craddock, J. P., Zheng, Y., Sun, Y., et al. (2020). Parallel extension tectonics: mechanism of early cretaceous thinning and destruction of the lithosphere of the North China craton. *Acta Petrol. Sin.* 36, 2331–2343. doi:10.18654/1000-0569/2020.08.04

Liu, J., Zhang, H., Sun, J., and Ye, J. (2004). Geochemical research on C-O and Sr-Nd isotopes of mantle-derived rocks from Shandong Province, China. *Sci. China Ser. D-Earth Sci.* 47, 171. doi:10.1360/02yd0432

Liu, X., Ding, Z., Bao, Z., Yan, C., Yu, H., Fan, J., et al. (2025). Geology, geochemistry and mineralization of the Taishang-Shuiwangzhuang supergiant gold deposit (>700 t Au), northwestern Jiaodong Peninsula, China: a review. *China Geol.* 8, 1–19. doi:10.31035/cg2023152

Liu, X., Fan, H., Evans, N. J., Yang, K., Danišík, M., McInnes, B. I. A., et al. (2017). Exhumation history of the Sanshandao Au deposit, Jiaodong: constraints from structural analysis and (U-Th)/He thermochronology. *Sci. Rep.* 7, 7787. doi:10.1038/s41598-017-08103-w

Liu, Y., Gao, S., Hu, Z., Gao, C., Zong, K., and Wang, D. (2009b). Continental and oceanic crust recycling-induced melt–peridotite interactions in the trans-north China orogen: U–Pb dating, Hf isotopes and trace elements in zircons from mantle xenoliths. *J. Petrol* 51, 537–571. doi:10.1093/petrology/egp082

Liu, Y., Hu, Z., Zong, K., Gao, C., Gao, S., Xu, J., et al. (2010). Reappraisement and refinement of zircon U-Pb isotope and trace element analyses by LA-ICP-MS. *Chin. Sci. Bull.* 55, 1535–1546. doi:10.1007/s11434-010-3052-4

Long, Z., Moynier, F., Debret, B., Qiu, K., Dai, W., and Sun, H. (2025a). Heavy potassium isotopes in carbonatites reveal oceanic crust subduction as the driver of deep carbon cycling. *Sci. Adv.* (in press).

Long, Z., Qiu, K., Halama, R., Yu, H., Zhang, J., Li, S., et al. (2025b). Reappraisal of potassium isotopic composition of the continental lithospheric mantle: insights from calc-alkaline lamprophyres in the eastern North China Craton. *Geol. Soc. Am. Bull.* doi:10.1130/B37952.1

Ma, C., and Li, Y. (2017). Incremental growth of granitoid plutons and highly crystalline magmatic differentiation. *Acta Petrol. Sin.* 33, 1479–1488.

Ma, Q., and Xu, Y. (2021). Magmatic perspective on subduction of Paleo-Pacific plate and initiation of big mantle wedge in East Asia. *Earth-Science Rev.* 213, 103473. doi:10.1016/j.earscirev.2020.103473

Ma, W., Fan, H., Liu, X., Pirajno, F., Hu, F., Yang, K., et al. (2017). Geochronological framework of the Xiadian gold deposit in the Jiaodong province, China: implications for the timing of gold mineralization. *Ore Geol. Rev.* 86, 196–211. doi:10.1016/j.oregeorev.2017.02.016

Maniar, P. D., and Piccoli, P. M. (1989). Tectonic discrimination of granitoids. *Geol. Soc. Am. Bull.* 101, 635–643. doi:10.1130/0016-7606(1989)101<0635:tdog>2.3.co;2

Martin, H. (1986). Effect of steeper Archean geothermal gradient on geochemistry of subduction-zone magmas. *Geology* 14, 753–756. doi:10.1130/0091-7613(1986)14<753:eosagg>2.0.co;2

Martin, H., Smithies, R. H., Rapp, R., Moyen, J.-F., and Champion, D. (2005). An overview of adakite, tonalite–trondhjemite–granodiorite (TTG), and sanukitoid: relationships and some implications for crustal evolution. *Lithos* 79, 1–24. doi:10.1016/j.lithos.2004.04.048

Moyen, J.-F. (2009). High Sr/Y and La/Yb ratios: the meaning of the "adakitic signature". *Lithos* 112, 556–574. doi:10.1016/j.lithos.2009.04.001

Ni, J., Liu, J., Tang, X., Yang, H., Xia, Z., and Guo, Q. (2013). The Wulian metamorphic core complex: a newly discovered metamorphic core complex along the Sulu orogenic belt, eastern China. *J. Earth Sci.* 24, 297–313. doi:10.1007/s12583-013-0330-5

Ni, J., Liu, J., Tang, X., Yang, H., Xia, Z., and Zhang, T. (2016). Early Cretaceous exhumation of the Sulu orogenic belt as a consequence of the eastern Eurasian tectonic extension: insights from the newly discovered Wulian metamorphic core complex, eastern China. *JGS* 173, 531–549. doi:10.1144/jgs2014-122

Ni, J., Liu, J., Wang, Y., Xia, Z., Ji, L., and Li, G. (2025). Control of the shift in subduction direction on upper plate tectonic extension and gold mineralization: a case study from the early cretaceous Jiaodong Peninsula, eastern China. *Tectonics* 44. doi:10.1029/2024TC008585

Ni, J., Wang, R., Liu, J., Wang, Z., Li, C., Ji, L., et al. (2024). Paleo-Pacific plate subduction direction change (122–118 Ma): insight from late kinematic plutons in the Wulian metamorphic core complex, Jiaodong Peninsula, eastern China. *Geol. Soc. Am. Bull.* 136, 3705–3734. doi:10.1130/B37080.1

Pang, J., Zheng, D., Ma, Y., Wang, Y., Wu, Y., Wan, J., et al. (2017). Combined apatite fission-track dating, chlorine and REE content analysis by LA-ICPMS. *Sci. Bull. (Beijing)* 62, 1497–1500. doi:10.1016/j.scib.2017.10.009

Pearce, J. A., Harris, N. B. W., and Tindle, A. G. (1984). Trace element discrimination diagrams for the tectonic interpretation of granitic rocks. *J. Petrol* 25, 956–983. doi:10.1093/petrology/25.4.956

Qiu, K., Deng, J., Laflamme, C., Long, Z., Wan, R., Moynier, F., et al. (2023a). Giant Mesozoic gold ores derived from subducted oceanic slab and overlying sediments. *Geochimica Cosmochimica Acta* 343, 133–141. doi:10.1016/j.gca.2023.01.002

Qiu, K., Deng, J., Sai, S., Yu, H., Tamer, M. T., Ding, Z., et al. (2023b). Low-temperature thermochronology for defining the tectonic controls on heterogeneous gold endowment across the Jiaodong Peninsula, eastern China. *Tectonics* 42. doi:10.1029/2022TC007669

Qiu, K., Romer, R. L., Long, Z., Williams-Jones, A. E., Yu, H., Turner, S., et al. (2024a). The role of an oxidized lithospheric mantle in gold mobilization. *Sci. Adv.* 10, eado6262. doi:10.1126/sciadv.ado6262

Qiu, K., Romer, R. L., Long, Z., Yu, H., Turner, S., Wan, R., et al. (2024b). Potassium isotopes as a tracer of hydrothermal alteration in ore systems. *Geochimica Cosmochimica Acta* 368, 185–196. doi:10.1016/j.gca.2024.01.005

Rapp, R. P., and Watson, E. B. (1995). Dehydration melting of metabasalt at 8–32 kbar: implications for continental growth and crust-mantle recycling. *J. Petrol* 36, 891–931. doi:10.1093/petrology/36.4.891

Reiners, P. W., and Brandon, M. T. (2006). Using thermochronology to understand orogenic erosion. *Annu. Rev. Earth Planet. Sci.* 34, 419–466. doi:10.1146/annurev.earth.34.031405.125202

Rickwood, P. C. (1989). Boundary lines within petrologic diagrams which use oxides of major and minor elements. *Lithos* 22, 247–263. doi:10.1016/0024-4937(89)90028-5

Sai, S., and Qiu, K. (2020). Ore-forming processes of the Rushan gold deposit, Jiaodong: fluid immiscibility induced by episodic fluid pressure fluctuations. *Acta Petrol. Sin.* 36, 1547–1566. doi:10.18654/1000-0569/2020.05.14

Song, M., Li, J., Li, S., Ding, Z., Tan, X., Zhang, Z., et al. (2018). Late mesozoic thermal upwelling-extension structure and its dynamics background in eastern shandong province. *J. Jilin Univ.* 48, 941–964. doi:10.13278/j.cnki.jjuese.20170145

Song, M., Li, J., Zhou, J., Song, Y., Li, S., Wang, B., et al. (2020a). The discovery and tectonic setting of the Early Cretaceous high-Mg diorites in the Jiaodong Peninsula. *Acta Petrol. Sin.* 36, 279–296. doi:10.18654/1000-0569/2020.01.22

Song, M., Wang, L., Song, Y., Li, J., Wang, B., Wei, X., et al. (2023). Geometry and origin of supergiant gold deposits in the Jiaodong gold province, eastern China. *J. Asian Earth Sci.* 254, 105744. doi:10.1016/j.jseaes.2023.105744

Song, M., Wang, S., Yang, L., Li, J., Li, S., and Ding, Z. (2017). Metallogenic epoch of nonferrous metallic and silver deposits in the Jiaodong Peninsula, China and its geological significance. *Acta Geol. Sin. Eng.* 91, 1305–1325. doi:10.1111/1755-6724.13363

Song, M., Yang, L., Fan, H., Yu, X., Ding, Z., Zhang, Y., et al. (2022). Current progress of metallogenic research and deep prospecting of gold deposits in the Jiaodong Peniusula during 10 years for Exploration Breakthrough Strategic Action. *Geol. Bull. China* 41, 903–935.

Song, M., Zhou, J., Song, Y., Wang, B., Li, S., Li, J., et al. (2020b). Mesozoic Weideshan granitoid suite and its relationship to large-scale gold mineralization in the Jiaodong Peninsula, China. *Geol. J.* 55, 5703–5724. doi:10.1002/gj.3607

Sun, H., Li, H., Liu, L., Chen, Q., Yang, H., and Wu, P. (2017). Exhumation history of the Jiaodong and its adjacent areas since the Late Cretaceous: constraints from low temperature thermochronology. *Sci. China Earth Sci.* 60, 531–545. doi:10.1007/s11430-016-0021-1

Sun, H., Wu, P., Li, H., Wang, Y., Danišík, M., Li, Z., et al. (2022). Comparison of the exhumed history and magnitude between Jiaojia and Linglong goldfields in the Jiaodong gold Province, North China: constraints from zircon and apatite (U-Th)/He data. *Ore Geol. Rev.* 144, 104857. doi:10.1016/j.oregeorev.2022.104857

Sun, W., and Li, S. (2023). Reconstruction of the Pacific plate: constraints from ocean floor and eastern China. *Innovation Geoscience* 1, 100013 EP. doi:10.59717/j.xinn-geo.2023.100013

Sun, X., and McDonough, W. F. (1989). *Chemical and isotopic systematics of oceanic basalts: implications for mantle composition and processes*, 42. Marylebone, London: Geological Society, London, Special Publications. 313–345 p.

Tang, J. (1998). Study on palaeogeothermal gradient and hydrocarbon generation in north China. *Petroleum Geol. Eng.* 12, 1-3+20–59.

Tong, H., Koyi, H., Huang, S., and Zhao, H. (2014a). The effect of multiple pre-existing weaknesses on formation and evolution of faults in extended sandbox models. *Tectonophysics* 626, 197–212. doi:10.1016/j.tecto.2014.04.046

Tong, H., Wang, J., Zhao, H., Li, B., Hao, H., and Wang, M. (2014b). Mohr space and its application to the activation prediction of pre-existing weakness. *Sci. China Earth Sci.* 57, 1595–1604. doi:10.1007/s11430-014-4860-1

Tong, H., and Yin, A (2011). Reactivation tendency analysis: a theory for predicting the temporal evolution of preexisting weakness under uniform stress state. *Tectonophysics* 503, 195–200. doi:10.1016/j.tecto.2011.02.012

Wang, B., Ding, Z., Bao, Z., Song, M., Zhou, J., Lv, J., et al. (2022). Mesozoic magmatic and geodynamic evolution in the Jiaodong Peninsula, China: implications for the gold and polymetallic mineralization. *Minerals* 12, 1073. doi:10.3390/min12091073

Wang, B., Ding, Z., Zhou, J., Qiu, K., and Sun, F. (2025a). Rapid tectonic transition, crust-mantle interaction, and gold metallogenesis in the Jiaodong Peninsula, eastern China: revealed by Early Cretaceous granitoids and microgranular mafic enclaves. *Lithos* 508-509, 108101. doi:10.1016/j.lithos.2025.108101

Wang, B., Song, M., Huo, G., Zhou, M., Xu, Z., Jiang, L., et al. (2021). Source characteristics and tectonic evolution of Late Mesozoic granites in Jiaodong and their implications for gold mineralization. *Acta Petrologica Mineralogica* 40, 288–320.

Wang, B., Song, M., Liu, Z., Li, J., Dong, L., Zhang, Y., et al. (2024a). Geochronology,Geochemical characteristics and tectonic implications of early cretaceous zhouguan high-Mg diorite rock mass in the Jiaodong Peninsula. *Gold Sci. Technol.* 32, 798–812. doi:10.11872/j.issn.1005-2518.2024.05.146

Wang, B., Zhou, J., Ding, Z., Wilde, S. A., Song, M., Zhao, T., et al. (2023). Late mesozoic magmatism and gold metallogeny of the Jiaodong Peninsula, China: a response to the destruction of the North China craton. *GSA Bull.* 136, 1395–1412. doi:10.1130/B37057.1

Wang, L., Yang, L., Yang, W., Zhi, Y., Xie, D., Sun, B., et al. (2025b). Genesis and exploration potential of gold deposits in Archean high-amphibolite facies metamorphic rocks of the Jiaodong Peninsula: geological and geochemical constraints from the Majiayao gold deposit. *Ore Geol. Rev.* 181, 106596. doi:10.1016/j.oregeorev.2025.106596

Wang, Q., Zhao, H., Yang, L., Groves, D. I., Han, J., Qiu, K., et al. (2025c). Formation of the giant Cretaceous Jiaodong-type orogenic gold province of the North China Craton: a consequence of lithospheric multi-layer reworking. *Geosci. Front.* 16, 102047. doi:10.1016/j.gsf.2025.102047

Wang, X., Wang, Z., Zhang, W., Ma, L., Chen, W., Cai, Y., et al. (2024b). Sulfur isotopes of lamprophyres and implications for the control of metasomatized lithospheric mantle on the giant Jiaodong gold deposits, eastern China. *GSA Bull.* 136, 3405–3418. doi:10.1130/B37274.1

Wang, Z., Yang, L., Guo, L., Marsh, E., Wang, J., Liu, Y., et al. (2015). Fluid immiscibility and gold deposition in the Xincheng deposit, Jiaodong Peninsula, China: a fluid inclusion study. *Ore Geol. Rev.* 65, 701–717. doi:10.1016/j.oregeorev.2014.06.006

Wen, B., Fan, H., Santosh, M., Hu, F., Pirajno, F., and Yang, K. (2015). Genesis of two different types of gold mineralization in the Linglong gold field, China: constrains from geology, fluid inclusions and stable isotope. *Ore Geol. Rev.* 65, 643–658. doi:10.1016/j.oregeorev.2014.03.018

Wu, F., Xu, Y., Zhu, R., and Zhang, G. (2014). Thinning and destruction of the cratonic lithosphere: a global perspective. *Sci. China Earth Sci.* 57, 2878–2890. doi:10.1007/s11430-014-4995-0

Wu, L., Monié, P., Wang, F., Lin, W., Ji, W., and Yang, L. (2018). Multi-phase cooling of early cretaceous granites on the Jiaodong Peninsula, east China: evidence from 40Ar/39Ar and (U-Th)/He thermochronology. *J. Asian Earth Sci.* 160, 334–347. doi:10.1016/j.jseaes.2017.11.014

Wu, X., and Zhu, G. (2024). Isostatic rising in the Linglong bivergent metamorphic core complex in the Jiaodong Peninsula: indication from kinematic vorticity. *Acta Geol. Sin.* 98, 31. doi:10.19762/j.cnki.dizhixuebao.2023116

Wu, X., Zhu, G., Yin, H., Su, N., Lu, Y., Zhang, S., et al. (2020). Origin of low-angle ductile/brittle detachments: examples from the cretaceous Linglong metamorphic core complex in eastern China. *Tectonics* 39. doi:10.1029/2020TC006132

Xia, Z., Liu, J., Ni, J., Zhang, T., Shi, X., and Wu, Y. (2016). Structure, evolution and regional tectonic implications of the Queshan metamorphic core complex in eastern Jiaodong Peninsula of China. *Sci. China Earth Sci.* 59, 997–1013. doi:10.1007/s11430-015-5259-3

Xu, J., Shinjo, R., Defant, M. J., Wang, Q., and Rapp, R. P. (2002). Origin of Mesozoic adakitic intrusive rocks in the Ningzhen area of east China: partial melting of delaminated lower continental crust? *Geology* 30, 1111–1114. doi:10.1130/0091-7613(2002)030<1111:oomair>2.0.co;2.CO;2

Xu, Y. (2001). Thermo-tectonic destruction of the archaean lithospheric keel beneath the sino-Korean craton in China: evidence, timing and mechanism. *Phys. Chem. Earth, Part A Solid Earth Geodesy* 26, 747–757. doi:10.1016/S1464-1895(01)00124-7

Xu, Z., Wang, Q., Tang, Z., and Chen, F. (2009). Fabric kinematics of the ultrahigh-pressure metamorphic rocks from the main borehole of the Chinese Continental Scientific Drilling Project: implications for continental subduction and exhumation. *Tectonophysics* 475, 235–250. doi:10.1016/j.tecto.2009.02.041

Yan, J., Chen, J. F., Xie, Z., Gao, T. S., Ka, F., Zhang, X. D., et al. (2005). Studies on petrology and geochernistry of the Later Cretaceous basalts and mantle-derived xenoliths from eastern Shandong. *Acta Petrol. Sin.* 21, 99–112.

Yang, F., Santosh, M., Glorie, S., Jepson, G., Xue, F., and Kim, S. W. (2020). Meso-cenozoic multiple exhumation in the shandong Peninsula, eastern north China craton: implications for lithospheric destruction. *Lithos* 370-371, 105597. doi:10.1016/j.lithos.2020.105597

Yang, K., Jiang, P., Fan, H., Zuo, Y., and Yang, Y. (2018). Tectonic transition from a compressional to extensional metallogenic environment at ~120 Ma revealed in the Hushan gold deposit, Jiaodong, North China Craton. *J. Asian Earth Sci.* 160, 408–425. doi:10.1016/j.jseaes.2017.08.014

Yang, K. F., Fan, H. R., Santosh, M., Hu, F. F., Wilde, S. A., Lan, T. G., et al. (2012). Reactivation of the Archean lower crust: implications for zircon geochronology, elemental and Sr–Nd–Hf isotopic geochemistry of late Mesozoic granitoids from northwestern Jiaodong Terrane, the North China Craton. *Lithos* 146-147, 112–127. doi:10.1016/j.lithos.2012.04.035

Yang, L., Deng, J., Wang, Z., Zhang, L., Goldfarb, R. J., Yuan, W., et al. (2016). Thermochronologic constraints on evolution of the Linglong Metamorphic Core Complex and implications for gold mineralization: a case study from the Xiadian gold deposit, Jiaodong Peninsula, eastern China. *Ore Geol. Rev.* 72, 165–178. doi:10.1016/j.oregeorev.2015.07.006

Yang, L., Deng, J., Zhang, L., Yang, W., Xie, D., Wang, L., et al. (2024). Jiaodong-type gold deposit. *Acta Petrol. Sin.* 40, 1691–1711. doi:10.18654/1000-0569/2024.06.01

Yang, W., Zhang, L., Zhang, B., Wang, S., Li, D., Ye, G., et al. (2023). Apatite fission-track thermochronology and magmatism-mineralization geochronology constraints on the tectono-thermal history of the Xiadian gold deposit, Jiaodong Peninsula, eastern China. *Acta Geol. Sin.* 39, 357–376. doi:10.18654/1000-0569/2023.02.05

Yao, M., Wu, H., Li, S., Liu, Y., Liu, S.-A., He, Y., et al. (2025). Formation of giant gold deposits driven by delamination of carbonated cratonic lithosphere. *Lithos* 506-507, 108070. doi:10.1016/j.lithos.2025.108070

Yin, J., Yuan, C., Sun, M., Long, X., Zhao, G., Wong, K. P., et al. (2010). Late Carboniferous high-Mg dioritic dikes in Western Junggar, NW China: geochemical features, petrogenesis and tectonic implications. *Gondwana Res.* 17, 145–152. doi:10.1016/j.gr.2009.05.011

Zhai, M., Fan, H., Yang, J., and Miao, L. (2004). Large-scale cluster of gold deposits in east shandong: anorogenic metallogenesis. *Earth Sci. Front.* 11, 85–98.

Zhang, J., Qiu, K., Yin, R., Long, Z., Feng, Y., Yu, H., et al. (2024). Lithospheric mantle as a metal storage reservoir for orogenic gold deposits in active continental margins: evidence from Hg isotopes. *Geology* 52, 423–428. doi:10.1130/G51871.1

Zhang, J., Zheng, Y., and Zhao, Z. (2009). Geochemical evidence for interaction between oceanic crust and lithospheric mantle in the origin of Cenozoic continental basalts in east-central China. *Lithos* 110, 305–326. doi:10.1016/j.lithos.2009.01.006

Zhang, L., Groves, D. I., Yang, L.-Q., Wang, G.-W., Liu, X.-D., Li, D.-P., et al. (2020). Relative roles of formation and preservation on gold endowment along the Sanshandao gold belt in the Jiaodong gold province, China: importance for province-to district-scale gold exploration. *Min. Deposita* 55, 325–344. doi:10.1007/s00126-019-00908-1

Zhang, L., Yang, L., Wang, Y., Weinberg, R. F., An, P., and Chen, B. (2017). Thermochronologic constrains on the processes of formation and exhumation of the Xinli orogenic gold deposit, Jiaodong Peninsula, eastern China. *Ore. Geol. Rev.* 81, 140–153. doi:10.1016/j.oregeorev.2016.09.026

Zhang, L., Yang, L., Weinberg, R. F., Groves, D. I., Wang, Z., Li, G., et al. (2019). Anatomy of a world-class epizonal orogenic-gold system: a holistic thermochronological analysis of the Xincheng gold deposit, Jiaodong Peninsula, eastern China. *Gondwana. Res.* 70, 50–70. doi:10.1016/j.gr.2018.12.013

Zhang, Q., Song, M., Ding, Z., Guo, M., Zhou, M., Dai, C., et al. (2022). Exhumation history and preservation of the Jiaojia giant gold deposit, Jiaodong Peninsula. *Sci. China Earth Sci.* 65, 1161–1177. doi:10.1007/s11430-021-9887-1

Zhang, Y., Dong, S., and Shi, W. (2003). Cretaceous deformation history of the middle Tan-Lu fault zone in Shandong Province, eastern China. *Tectonophysics* 363, 243–258. doi:10.1016/S0040-1951(03)00039-8

Zhang, Y., Li, J., Zhang, T., Dong, S., and Yuan, J. (2008). Cretaceous to Paleocene tectono-sedimentary evolution of the Jiaolai basin and in the contiguous areas of Shandong peninsular (North China) and geodynamic implications. *Acta Geol. Sin.*, 1229–1257.

Zhao, D. (2004). Origin of the Changbai intraplate volcanism in Northeast China: evidence from seismic tomography. *Chin. Sci. Bull.* 49, 1401. doi:10.1360/04wd0125

Zhao, R. U., Wang, Q., Liu, X., Santosh, M., Yuan, W., and Wang, W. E. (2018). Uplift history of the Jiaodong Peninsula, eastern North China Craton: implications for lithosphere thinning and gold mineralization. *Geol. Mag.* 155, 979–991. doi:10.1017/S0016756816001254

Zheng, Y., and Wu, F. (2009). Growth and reworking of cratonic lithosphere. *Sci. Bull.* 54, 3347–3353. doi:10.1007/s11434-009-0458-y

Zheng, Y., Xu, Z., Zhao, Z., and Dai, L. (2018). Mesozoic mafic magmatism in North China: implications for thinning and destruction of cratonic lithosphere. *Sci. China Earth Sci.* 61, 353–385. doi:10.1007/s11430-017-9160-3

Zhu, R., Fan, H., Li, J., Meng, Q., Li, S., and Zeng, Q. (2015). Decratonic gold deposits. *Sci. China Earth Sci.* 58, 1523–1537. doi:10.1007/s11430-015-5139-x

Zhu, R., and Sun, W. (2021). The big mantle wedge and decratonic gold deposits. *Sci. China Earth Sci.* 64, 1451–1462. doi:10.1007/s11430-020-9733-1

Zhu, R., and Xu, Y. (2019). The subduction of the west Pacific plate and the destruction of the North China Craton. *Sci. China Earth Sci.* 62, 1340–1350. doi:10.1007/s11430-018-9356-y

Zhu, R., and Zheng, T. (2009). Destruction geodynamics of the North China craton and its Paleoproterozoic plate tectonics. *Sci. Bull.* 54, 3354–3366. doi:10.1007/s11434-009-0451-5